INVESTIGATION OF ON-SITE DIAGNOSTIC TESTING TECHNIQUES FOR METAL OXIDE SURGE ARRESTERS

By

HANXIN ZHU

A Thesis

Submitted to the Faculty of Graduate Studies

In Partial Fulfillment of the Requirements

For the Degree of

Master of Science

Department of Electrical and Computer Engineering
University of Manitoba
Winnipeg, Manitoba
© Hanxin Zhu, April 2000

National Library of Canada

Acquisitions and Bibliographic Services

395 Wellington Street
Ottawa ON K1A 0N4
Canada

Bibliothèque nationale du Canada

Acquisitions et services bibliographiques

395, rue Wellington
Ottawa ON K1A 0N4
Canada

Your file Votre référence

Our file Notre référence

The author has granted a non-exclusive licence allowing the National Library of Canada to reproduce, loan, distribute or sell copies of this thesis in microform, paper or electronic formats.

L'auteur a accordé une licence non exclusive permettant à la Bibliothèque nationale du Canada de reproduire, prêter, distribuer ou vendre des copies de cette thèse sous la forme de microfiche/film, de reproduction sur papier ou sur format électronique.

The author retains ownership of the copyright in this thesis. Neither the thesis nor substantial extracts from it may be printed or otherwise reproduced without the author's permission.

L'auteur conserve la propriété du droit d'auteur qui protège cette thèse. Ni la thèse ni des extraits substantiels de celle-ci ne doivent être imprimés ou autrement reproduits sans son autorisation.

0-612-51829-9

Canada

THE UNIVERSITY OF MANITOBA

FACULTY OF GRADUATE STUDIES

*****

COPYRIGHT PERMISSION PAGE

Investigation of On-site Diagnostic Testing Techniques for Metal Oxide Surge Arresters

BY

Hanxin Zhu

A Thesis/Practicum submitted to the Faculty of Graduate Studies of The University

of Manitoba in partial fulfillment of the requirements of the degree

of

Master of Science

HANXIN ZHU © 2000

Permission has been granted to the Library of The University of Manitoba to lend or sell copies of this thesis/practicum, to the National Library of Canada to microfilm this thesis/practicum and to lend or sell copies of the film, and to Dissertations Abstracts International to publish an abstract of this thesis/practicum.

The author reserves other publication rights, and neither this thesis/practicum nor extensive extracts from it may be printed or otherwise reproduced without the author's written permission.

ACKNOWLEDGEMENTS

I would like to express my profound gratitude to my supervisor, Dr. M.R. Raghuveer for his invaluable guidance, enthusiasm, and encouragement in this study. Dr. Raghuveer did not only supervise me in this research but also set up an example of a scientist and a thinking engineer. His rigorous scientific approach and strict demand on the research encouraged me to have fulfilled the requirements of this thesis.

Funding from Manitoba Hydro and partial funding from NSERC, Canada is gratefully acknowledged.

I appreciate and acknowledge Mr. W.McDermid and Mr. Ahmed Glodjo for their invaluable input in this work.

I would also like to thank Mr. John Kendall for his technical help on numerous occasions during the course of this work.

Finally, I would like to dedicate this thesis to my parents, my wife and my son for their encouragement, support, understanding and assistance.

ABSTRACT

Metal Oxide Surge Arresters (MOSA) degrade in service due to the combined effects of transient overvoltage, temperature and moisture ingress. As a MOSA ages, its resistive leakage current increases with accompanying increase in the third harmonic component, which is used as indicator of ageing in the probe method, the compensation method and neutral current method. Test errors with these three most widely used on-site diagnostic test techniques are investigated in this thesis.

Test error associated with probe method is due to its inherent assumptions. In this method, researchers have developed a technique to account for the third harmonic component of capacitive current in deriving the resistive third harmonic current from the leakage current. However, the influence of voltage harmonics on the magnitude of the resistive current has not been considered which aspect is explored in this thesis. The introduction of the probe and an assumption of a constant field factor will also result in errors. This aspect will be verified by the laboratory test results.

In the compensation method, the capacitive current is directly compensated by the introduction of the system voltage. But, the existence of voltage harmonics and interphase interferences will render the criteria of compensation invalid and thus result in the uncompleted compensation of the capacitive current. To improve this method for field use, the criteria of compensation should be modified and a soft phase shifter should be introduced as discussed in this thesis.

It is known that by using neutral current method for on-site test one can not tell the real condition of three phase MOSA. In order to enable its use as a diagnostic indicator, slight modifications, discussed in fair detail in this thesis, are necessary.

Finally, test results show that the simplified representation model of MOSA is questionable. This aspect is also briefly discussed.

The results of this investigation could be applied to on-site diagnostic test of MOSA. The proposals made for improving the compensation method and the neutral current method may be realized and should be implemented for future use.

SYMBOLS, DEFINITIONS, UNITS AND TYPICAL VALUES OF PARAMETERS

English Symbols

Symbol	Definition	Unit	Typical Value
L	Inductance of metal oxide disc	H	
R_z	Resistance of ZnO grains	Ω	
R_i	Resistance of the granular layers	Ω	
C	Capacitance between granular layers	F	
i_t	Total current of MOSA	mA	
i_c, I_c	Capacitive current of MOSA	mA	1mA
i_r, I_r, I_R	Resistive leakage current of MOSA	mA	200μA
V_s	System voltage	kV	
V_{s0}	System voltage with 90°shift ahead	kV	
G	Constant corresponds to ωC		
$V_{a,b,c}$	Phase to ground voltage of phase A,B,C	kV	
C_{ab}	Stray capacitance between phase A and B	F	
C_{bc}	Stray capacitance between phase B and C	F	
I_{ca}	Capacitivecurrent of phase A	mA	
I_{cba}	Coupling current from phase B to phase A	mA	
I_{cax}	Phasor sum of I_{ca} and I_{cba}	mA	
V_I	Input voltage of the phase shifter	kV	
V_O	Output voltage of the phase shifter	kV	

G'	Constant corresponds to ωC	
I_0	Neutral current	mA
I_{r3}	3rd harmonic resistive current	mA
I_{t3}	Total 3rd harmonic leakage current	mA
I_{c3}	3rd capacitive harmonic current	mA
I_{p1}	Fundamental component of the Probe current	mA
I_{t1}	Fundamental component of total current	mA
I_{p3}	3rd harmonic of the probe current	mA
I_{t3}	3rd harmonic of total current	mA
k_1	Ratio of I_{t1} to I_{p1}	
k_3	Ratio of I_{t3} to I_{p3}	
t	Time	second
i'_{r3}	Resistive 3rd harmonic current due to voltage harmonics	mA
V_3	3rd harmonic voltage	kV
V_5	5th harmonic voltage	
V_7	7th harmonic voltage	
V_N	Rated voltage of MOSA	kV
v_n	nth harmonic voltage	
i_{cn}	nth harmonic capacitive current	mA
i_{rn}	nth harmonic resistive current	mA
v_{1s0}	Fundamental component of v_{s0}	kV

Greek Symbols

ρ	Resistivity	Ωm	
ε_r	Relative dielectric constant		
α	Rate of change of $\ln i_r$ with respect to $\ln v$		
τ	discretized time interval	second	
ω	Angular frequency	rad/s	376.8
Φ_3	Phase angle of 3^{rd} harmonic voltage	rad	
Φ_5	Phase angle of 5^{th} harmonic voltage	rad	

LIST OF FIGURES

Fig.	Title	Page
1.1	Typical V-I Characteristics of a typical metal oxide disc	1
1.2	Equivalent representation of MOSA	3
1.3	Schematic diagram of the resistive leakage current measuring instrument	7
1.4	Phasor diagram showing the influence of the neighbouring phases	8
1.5	Schematic diagram of a phase shifter	9
1.6	Probe method	12
1.7	Schematic diagram of neutral current method	14
2.1	120kV MOSA voltage-resistive current i_r relation	20
2.2	120kV MOSA voltage v-resistive current i_r relation	21
2.3	Spectrum of resistive harmonic current in unaged 120kV MOSA for pure sinusoidal applied voltage	23
2.4	v-i_r characteristics of aged and unaged MOSA	24
2.5	Spectrum of resistive harmonic current in an aged 120kV MOSA for pure sinusoidal applied voltage	25
2.6	Spectrum of resistive harmonic current in unaged 120kV MOSA for applied voltage contaminated with 3% of 3rd harmonic voltage, Φ_3=0°	27
2.7	Spectrum of resistive harmonic current in unaged 120kV MOSA for applied voltage contaminated with 3% of 3rd harmonic voltage, Φ_3=180°	28

Fig.	Title	Page
2.8	Showing dependence of resistive 3rd harmonic current on 3rd	

	harmonic voltage, V_3, and its phase angle, Φ_3	29
2.9	Spectrum of resistive harmonic current in unaged 120kV MOSA for applied voltage applied voltage contaminated with 2% of 5^{th} harmonic voltage, Φ_5=0°	30
2.10	Spectrum of resistive harmonic current in unaged 120kV MOSA for applied voltage applied voltage contaminated with 2% of 5^{th} harmonic voltage, Φ_5=180°	30
2.11	Showing dependence of resistive 3^{rd} harmonic current on 5^{th} harmonic voltage V_5, and its phase angle, Φ_5	31
2.12	Spectrum of resistive harmonic current in unaged 120kV MOSA for applied voltage contaminated with 3% of 3^{rd} and 2% of 5^{th} harmonic voltage components, Φ_3=0°,Φ_5=0°	32
2.13	Spectrum of resistive harmonic current in unaged 120kV MOSA for applied voltage contaminated with 3% of 3^{rd} and 2% of 5^{th} harmonic voltage components, Φ_3=0°,Φ_5=180°	33
2.14	Spectrum of resistive harmonic current in unaged 120kV MOSA for applied voltage contaminated with 3% of 3^{rd} and 2% of 5^{th} harmonic voltage components, Φ_3=180°,Φ_5=0°	34
2.15	Spectrum of resistive harmonic current in unaged 120kV MOSA for applied voltage contaminated with 3% of 3^{rd} and 2% of 5^{th} harmonic voltage components, Φ_3=180°,Φ_5=180°	34
Fig.	Title	Page
2.16	Spectrum of resistive harmonic current in unaged 120kV MOSA for	

applied voltage contaminated with 5% of 3rd and 5th harmonic voltage components, Φ_3=0°,Φ_5=180° 35

3.1 Circuit to determine MOSA parameters 39

3.2 V-I characteristic curves of the tested MOSA valve elements 41

3.3 Schematic diagram of single phase laboratory set-up to obtain MOSA leakage current 42

3.4 Simplified electrical representation of MOSA 43

3.5 Waveshapes of MOSA applied voltage and total leakage current, V.E.#10&#14 in series 45

3.6 Showing calculation for the equivalent C of MOSA set 46

3.7 Showing the waveshapes of applied voltage, capacitive and resistive leakage currents of MOSA(V.E. #14&#16) 47

3.8 Spectrum of the applied voltage and i_r 47

3.9 Average v-i_r characteristics curves of aged and unaged MOSA sets 48

3.10 Probe method proposed in [LUN90] 51

3.11 Laboratory setup for three-phase test of MOSA 53

3.12 Capacity probe and plate to hold the probe 54

3.13 Wave shapes of the leakage current and the probe current obtained with the probe located at 0° under phase A (left most phase) 55

3.14 Neutral current and the applied voltage (11kV) in phase A, MOSA in all three phases unaged 59

Fig.	Title	Page
3.15	Phase A voltage and neutral current with aged MOSA in phase C	60
3.16	The waveshape of the applied voltage (MCOV) and total Current	62
3.17	Measurement necessary for use of neutral current method as a Diagnostic indicator	63
3.18	Suggested test circuit for the use of the neutral current method as A diagnostic indicator	64
3.19	Waveshapes of the applied voltage and leakage currents	65
3.20	v-i_r characteristics of the MOSA from test results	66
3.21	Waveshapes of the simulated and measured neutral currents of Unaged MOSA in a three phase system	67
3.22	Measured and simulated neutral currents with aged MOSA In phase C	68

LIST OF TABLES

Table	Title	Page
2.1	Summary of simulation results	32
2.2	Simulation results for unaged MOSA	36
3.1	Test data of MOSA valve elements #1 to #16	40
3.2	I_r and I_{r3} of MOSA sets	48
3.3	Test results, probe method	55
3.4	Third harmonic current after interchange of MOSA columns in phase A and C	57

TABLE OF CONTENTS

ACKNOWLEDGEMENT i

ABSTRACT ii

Symbols, Definition, Units and Typical Values of Parameters iii

LIST OF FIGURES vi

LIST OF TABLES x

Table of Contents xi

Chapter 1 **INTRODUCTION** 1

1.1 Deterioration of MOSA 4

1.2 An Introduction to Existing On-site Diagnostic Testing Techniques 5

1.2.1 Total Current Method 5

1.2.2 Resistive Leakage Current and Power Loss Method 6

1.2.2.1 The principle of the resistive leakage current and power loss method 6

1.2.2.2 Error Associated with resistive leakage current and power loss method 8

1.2.3 Probe Method 11

1.2.3.1 Principle of probe method 11

1.2.3.2 Test error with probe method 13

1.2.4 Neutral Current Method 14

1.2.4.1 The principle of neutral current method 14

1.2.4.2 Error associated with neutral current method

14

1.3 Scope of present investigation 15

1.3.1 Study of the influence of harmonic voltage on on-site testing of MOSA 16

1.3.2 Investigation of the techniques for on-site diagnostic testing of MOSA 16

1.3.3 Brief discussion of the simple representative model of MOSA 16

Chapter 2 **INFLUENCE OF VOLTAGE HARMONICS ON MOSA RESISTIVE CURRENT USED AS A DIAGNOSTIC INDICATOR** 17

2.1 Representation of MOSA v-i_r Characteristics in the Low Electric Field Region 19

2.1.1 Exponential Representation 19

2.1.2 Polynomial Representation 21

2.2 Harmonic Components of Resistive Current of Aged and Unaged MOSA under Pure Sinusoidal Applied Voltage 22

2.2.1 Case 1: Unaged MOSA, Pure Sinusoidal Applied Voltage 22

2.2.2 Case 2: Aged MOSA, Pure Sinusoidal Applied Voltage 24

2.3 Harmonic Content of Voltage in Power System 25

2.4 Effect of Nonsinusoidal Voltage on Harmonic Components of the Resistive Current of the Unaged 120kV MOSA 26

2.4.1 Effects of 3rd Harmonic in Voltage on the 3rd Harmonic Component of Resistive Leakage Current 26

2.4.2 Effects of 5th Harmonic Voltage on Spectral Components of the Resistive Leakage Current 29

2.4.3 Influence of Combined 3rd and 5th Harmonic Voltage on the 3rd Harmonic Component of the Leakage Current 31

2.5 Summary of the Simulation Results for Unaged MOSA 36

Chapter 3 **INVESTIGATION OF ON-SITE DIAGNOSTIC TESTING TECHNIQUES OF MOSA** 38

3.1 Investigation of the v-i_r Characteristics of MOSA 38

3.2 On-site Diagnostic Test Method Comparison Strategy 41

3.3 Compensation Technique 42

3.3.1 Application of Compensation Technique to Obtain the Capacitance Of MOSA Elements; Single Phase System 45

3.3.2 Diagnostic Indicator Obtained From Direct Method on a One-phase System; Benchmark Method 46

3.3.3 MOSA Diagnostics in a Three Phase System Utilizing the Compensation Technique 49

3.4 Investigation of On-site Diagnostic Testing Techniques of MOSA 50

3.4.1 Principle of the Probe Method 50

3.4.2 Laboratory Setup for Verification of Probe Method 53

3.4.3 Comparing Results from Probe Method with the Benchmark Method 54

3.4.4 Brief Comments on the Probe Method 57

3.5 Neutral Current Method 58

3.5.1 MOSA in All Three Phases Unaged 58

3.5.2 Aged MOSA set in Phase C, Unaged Sets in the Other Phases 59

3.5.3 Comments on Neutral Current Method 60

3.5.4 Use of Neutral Current Method as a Diagnostic Indicator 61

3.5.5 Necessary Modification to the Neutral Current Method to Enable

Its Use as a Diagnostic Indicator 61

3.6 Discussion of Electrical Representation Models of MOSA 64

3.6.1 v-i_r Characteristics of MOSA from Test Results 65

3.6.2 Comparison of Test and Simulation Results, Neutral Current Method 66

3.6.3 Effect of MOSA Representation on Simulation Results 68

Chapter 4 **CONCLUSIONS** 69

4.1 Conclusion 69

4.2 Recommendation for Future Research 70

REFERENCES 72

Chapter 1

Introduction

Metal oxide arrester valve elements (MOSA) consist primarily of zinc oxide and other selected metal oxide additives. When examined under an electron microscope, it is seen that the low resistive Zinc Oxide grains are surrounded and separated by a strongly bonded high resistive oxide granular layer, which serves to produce the desired highly non-linear resistive characteristics, shown in Fig.1.1.

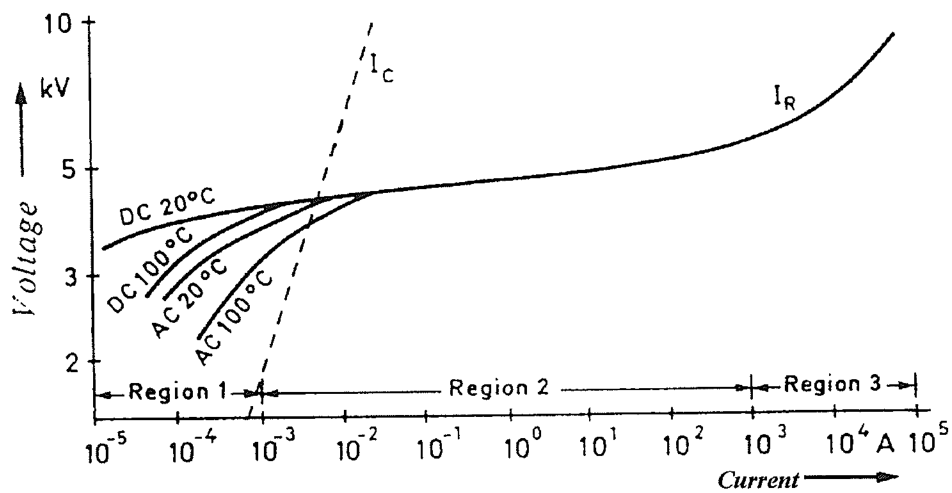

Figure 1.1: Typical V-I Characteristics of a typical metal oxide disc (80mm diameter, 20mm height) [1].

Note: ac voltage is the instantaneous value.

As shown in Fig.1.1, the characteristics of the resistive leakage current may be divided into three regions, i.e. the low electric field region (region 1), the medium electric field region (region 2) and the high electric field region (region 3).

In the low electric field region, the current is dominated by the capacitive component. The resistive component depends not only on the applied voltage, but also on the temperature. It can also be seen from Fig.1.1 that the V-I characteristics of a MOSA element is remarkably different under dc and ac applied voltages in the low voltage region. This suggests quite different conducting mechanisms in these two cases. Usually, the conduction mechanism of MOSA is explained by consideration of energy barriers in the granular layers [2]. According to this theory, the barriers prevent movements of electrons from one grain to another; but Schottky emission causes a small current flow through the material and this current is the resistive leakage current. A higher temperature causes higher electron energy and in turn causes more electrons to pass over the barrier. The V-I characteristic curves shown in Fig.1.1 reinforce this explanation.

In the middle and high electric field regions, the conduction mechanism of MOSA can be explained by the tunnel-effect and reversed-biased Schottky emission respectively. The voltage drop across the resistor R_z (Fig.1.2) will gradually dominate and the V-I characteristic curve will approach linearity [1].

In order to keep the power dissipation in a MOSA small when it operates in the normal state, the continuous operating voltage (MCOV) of the MOSA is chosen in the low voltage region. The protection characteristics of the MOSA are determined by the v-i characteristics in Medium and High Electric field regions, and the influences of the capacitive component and temperature disappear in these regions.

The non-linear V-I characteristics of a MOSA valve element is usually represented by the equivalent circuit shown in Fig.1.2 [1]. In Fig.1.2, R_i represents the non-linear resistance of the granular layers, whose resistivity ρ changes from 10^8 Ωm for low electric stress to just below 0.01 Ωm for high electric stress. The resistor, R_z, with a much lower resistance value than R_i at below 0.01 Ωm, represents the resistance of the Zinc Oxide grains. The equivalent capacitor C represents the capacitance between the granular layers with a relative dielectric constant between 500-1200. The inductance L represents the inductance of the metal oxide disc and is determined by the geometry of the current flow path. As R_z<<R_i, the influence of R_z is often neglected in normal operation.

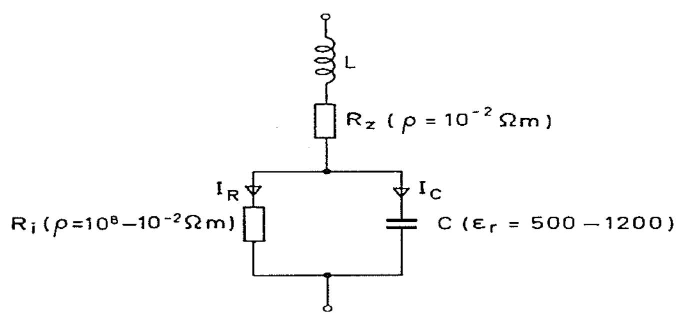

Figure 1.2. Equivalent representation of MOSA [1]

1.1. Deterioration of MOSA

MOSA degrades in service under the influence of constant working voltage, internal partial discharges, uneven heating and solar irradiation, possible moisture ingress and the occurrence of transient over-voltage; all of the above result in an increased value of resistive leakage current.

Internal partial discharges cause degradation of MOSA. It is known that some gases may be formed in service because of partial discharge inside the MOSA housing. The granular layer of MOSA reacts chemically with the surrounding unstable gas molecules, which results in the deterioration of the electrical property of the combination of ZnO and its granular layers. To limit this effect, measures may be taken in the process of selection of MOSA and sealing techniques.

Uneven heating and irradiation also degrades MOSA. A simple example of these effects is due to the heat from the sun. In service, a MOSA will not be evenly warmed; the warming effect also varies from season to season. The hot portion of the MOSA will draw more leakage current as compared with the cold portion. This causes non-uniformity of current distribution and ageing.

A high transient voltage, hence a high current stress on MOSA, will cause the degradation of MOSA too. High current through MOSA results in an excessive local current density through the granular layers, and this may partially destroy them.

Thus, with the passage with time, a MOSA may exhibit ageing. The aged MOSA manifests itself in an increased component of resistive leakage current, especially the 3^{rd} harmonic component. A serious consequence of this increased leakage current is that the energy absorption capability decreases which in turn may lead to thermal runaway and cause failure of MOSA. Therefore, it is very important to periodically check the condition of MOSA in service to ensure that its operating characteristics are acceptable.

1.2. An Introduction to Existing On-site Diagnostic Testing Techniques

Over the years, diagnostic testing techniques have been proposed, which are based on the measurement of radio interference, partial discharge and emitted electromagnetic radiation. These methods, because of interference from other sources on-site, cannot detect the real operating condition of MOSA.

On the other hand, diagnostic testing techniques based directly on the measurement of leakage current have offered the most promise. These methods which are currently widely used for on-site diagnostics include: measurement of the total leakage current, the resistive leakage current, higher order harmonic currents in the leakage current and the zero sequence current measuring method.

1.2.1. Total Leakage Current Method [3, 4]

This is a method commonly implemented by means of a permanently installed milliampere meter in the ground connection of a MOSA. The reading of this meter indicates the total current I_t.

As shown in Fig.1.2,

$$i_t = i_c + i_r \tag{1-1}$$

The degradation of a MOSA results in the increase of its resistive leakage current i_r, and hence the total leakage current i_t. This will result in an increased reading of the milliampere meter. Thus, the condition of a MOSA can be assessed from the reading of this meter.

However, experience tells us that this method is not sensitive to the change in the magnitude of the resistive leakage current. Depending on the diameter of the MOSA discs, the peak value of the capacitive current of MOSA ranges from 0.5 to 3mA. The capacitive current of a MOSA depends on the number of valve elements in parallel, the stray capacitance between the MOSA column and other MOSA or charged objects and the voltage applied across the MOSA. The resistive leakage current component, on the other hand, is in the range of 50-500 μA (peak), depending on the temperature, applied voltage and the condition of a MOSA.

Suppose that for an unaged MOSA, its original resistive leakage current is 50μA and that the capacitive component is 1 mA. Suppose now that the MOSA ages and the resistive leakage current reaches a value of 500μA, which is an increase of 1000% in the resistive leakage current; the corresponding increase in the reading of the milliampere meter is only 10%. According to operating experience, an obvious change in the reading of the milliampere meter will be noticed only if moisture ingress is very serious or the MOSA has aged considerably. This method fails as a diagnostic method if the arrestor is aged only slightly. Therefore, this method is unsuitable for on-site checks of the condition of MOSA.

1.2.2. Resistive Leakage Current and Power Loss Method [5, 6]

In order to investigate the ageing process of MOSA, a compensation method, which uses the resistive leakage current I_r and power loss P as indicators, has been proposed.

1.2.2.1. The Principle of the Resistive Leakage Current and Power Loss Method

The structure of this kind of instrument is illustrated in Fig.1.3.

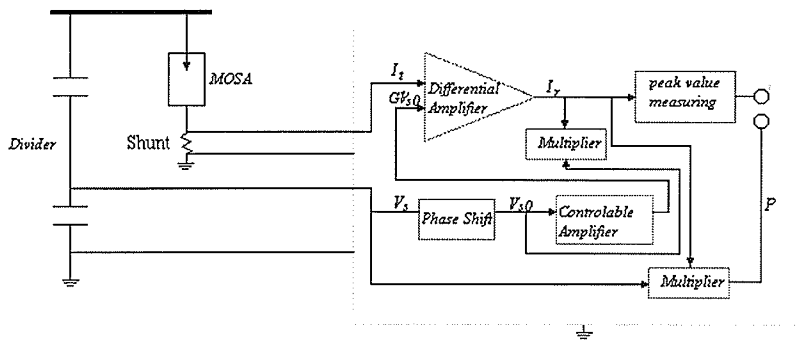

Figure 1.3. Schematic diagram of the resistive leakage current measuring instrument [4].

Two channels of signals, the total current I_t and the system voltage V_s, are obtained from a CT and a voltage divider (or a PT) respectively. The voltage V_s is shifted 90° ahead in order to keep it in phase with the capacitive component of I_t. The phase shifted voltage signal V_{s0} is then sent to the controllable amplifier. The output GV_{s0} is input into a differential amplifier and to obtain the signal (I_t - GV_{s0}). The amplifier and the multiplier form an automatic feedback system to control the controllable amplifier.

Suppose that V_s is purely sinusoidal, the value of G is changed until the magnitude of (I_c-GV_{s0}) reaches zero, i.e. the capacitive component in I_t has been completely compensated; the resistive component, I_r, which equals to (I_t-GV_{s0}), can then be obtained. The peak value of I_r and the power loss P can be obtained through a peak value measurement unit and a multiplier and can be displayed.

1.2.2.2. Errors Associated With Resistive Leakage Current and Power Loss Method

The resistive leakage current and power loss method is a quite straightforward method. For on-site monitoring, the errors associated with it are due to the following aspects.

First, errors result due to inter-phase interference.

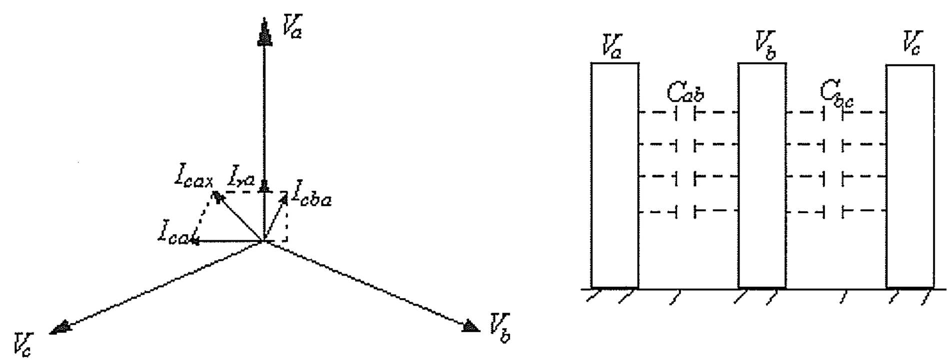

Figure 1.4. Phasor diagram showing the influence of the neighbouring phases

Fig.1.4 shows the phasor diagram of three-phase voltages and phase A current. I_{ra} is the resistive leakage current component of phase A, and I_{ca} is the capacitive current component while I_{cba} is the current coupled through C_{ab} from the neighbouring phase B. In this case, we suppose that the MOSA works under pure sinusoidal voltage. The phasor sum of I_{ca} and I_{cba} is I_{cax}, which lags I_{ca}. The phasor I_{cax} is not at 90° with respect to V_a. If the compensation criteria mentioned above is implemented, the capacitive current can not be totally compensated for and a larger resistive reading will be obtained for phase A.

Measurements in phases B and C may be analysed similarly. The resistive leakage current in the middle phase, phase B, will not be influenced by the neighbouring phases while the value in phase C will be lower than its real value.

In order to exclude the influence of neighbouring phases, a phase shifter [5] [7], as shown in Fig.1.5, was introduced, which is inserted ahead of the testing instrument for on-site diagnostic testing.

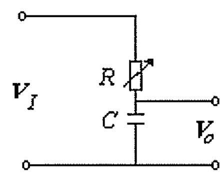

Fig.1.5. Schematic diagram of a phase shifter [5] [7]

Let the input voltage be V_I, and the output voltage from the phase shifter be V_O. Then,

$$\bar{V}_O = \left[\frac{1}{j\omega C} / (R + \frac{1}{j\omega C})\right]\bar{V}_I = \bar{V}_I(1 + (\omega CR)^2)^{-\frac{1}{2}}\angle - arctg(\omega CR) \quad (1\text{-}2)$$

As mentioned above, the phase angle of the capacitive current will change because of the influence of the neighbouring phase. Since the coupling current is quite small compared with I_{ca}, the change in phase angle should be very small. The magnitude of the shift in the angle is given by Eq.1-3.

$$\theta = -arctg(\omega CR) \approx -\omega CR \quad (1\text{-}3)$$

and the shift in angle of the n^{th} order harmonic component will be n times the shift of the fundamental component. Due to the insertion of the phase shifter, the change in magnitude is given by $(1+(\omega CR)^2)^{-\frac{1}{2}} \approx 1$, i.e. the magnitude after shifting is almost the same as the pre-shift magnitude.

After shifting of the phase angle, by selecting a suitable G′, the value of (I_{cax}-$G'Vs0$) may be made to equal zero. The resistive leakage current can then be calculated as

$$I_r = I_t - G'V_{s0} \tag{1-4}$$

In Eq.1-4, I_t is the total leakage current, which includes interphase interference.

The second aspect of error introduced from the measurement is from harmonic voltages. This influence manifests itself in two ways.

On the one hand, as will be discussed in Chapter 2, the harmonic voltages, their magnitude and phase angle, will greatly influence the value of I_r and will cause very misleading results.

On the other hand, as discussed above, if a phase shifter and the testing instrument are used together, test errors will result as well. Suppose that the system voltage comprises of the fundamental, 3rd and 5th harmonic voltages only. The magnitude of the phase angle shift can be obtained from Eq.1-3. For higher order harmonics, the phase shift angle will be n times that of the fundamental component. But, for the zero sequence 3rd harmonic voltage component, its phase angle does not need shifting; and for the negative 5th harmonic voltage component, its phase angle should be shifted in the opposite direction, and the magnitude of the shifting angle will not be linear with that of the fundamental component. Thus, a fixed phase shifter will cause an incomplete compensation of the total capacitive component.

Finally, the errors, especially the phase angle error, introduced by the clamp type CT should not be neglected.

In order to minimize the influences mentioned above, this technique needs some modification which will be discussed in Chapter 3.

1.2.3. Probe Method [3]

This is a compensation technique originally proposed by Scandinavian researchers [3]. It uses the 3rd harmonic component of the resistive leakage current as the indicator. An instrument based on this technique is manufactured by a Norwegian company and is still in use. According to the company's internet advertisement of this instrument [http://www.Transinor.st.no/products/lcm/teclcm. html], this instrument is not sensitive to system harmonics, and the test result will not be influenced by the position of the probe. As discussed in Chapters 2 and 3, these claims may be misleading.

1.2.3.1. Principle of Probe Method

The schematic diagram of this method is shown in Fig.1.6. A detailed discussion of this method has been included in chapter 3.

As shown in Fig.1.6, from the ground connection of MOSA, the total current I_t can be obtained with a shunt or a clamp type CT. The probe current I_p, on the other hand, can be obtained by introducing a capacitive probe.

The capacitive current should be known to enable the calculation of I_{r3} as shown in Eq.1-4.

$$\bar{I}_{r3} = \bar{I}_{t3} - \bar{I}_{c3} \tag{1-4}$$

Because of the difficulties in obtaining the capacitive current component directly, the probe current is used to derive I_{c3} in Eq.1-4 by introduction of the ratio of two factors, k_1 and k_3.

$$k_1 = {}^{I_{t1}}\!\big/_{I_{p1}} \tag{1-5}$$

and

$$k_3 = {}^{I_{t3}}\!\big/_{I_{p3}} \tag{1-6}$$

In Eqs.1-5 and 1-6. I_{t1}, I_{t3} are the fundamental and 3rd harmonic leakage currents, and I_{p1} and I_{p3} are the fundamental and 3rd harmonic probe currents.

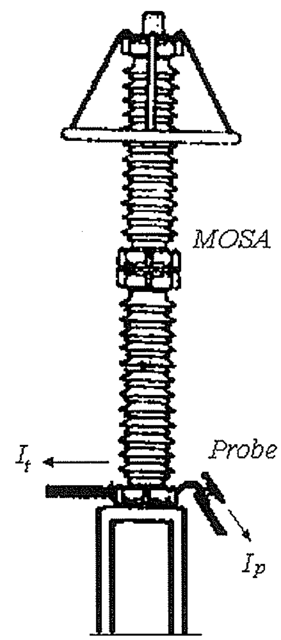

Figure 1.6 Probe Method [3]

It is implied that although k_1 and k_3 are sensitive to the configuration of MOSA, their ratio may be practically constant. The value of this ratio, according to a Boundary Element Method simulation, is in the range of 0.69-0.82 for a variety of

MOSA configurations as illustrated in [3]. Taking the average of this ratio, I_{r3} can be calculated from Eq.1-7.

$$\bar{I}_{r3} = \bar{I}_{t3} - 0.75\bar{I}_{p3}\frac{I_{t1}}{I_{p1}} \quad (1\text{-}7)$$

1.2.3.2. Test Error Inherent with Probe Method

The probe picks up the 3rd harmonic voltage component, which is then used to compensate for the influence of the 3rd harmonic voltage. As shown in Chapter 2, in detail, the 3rd harmonic resistive leakage current component will not only be influenced by the fundamental and 3rd harmonic voltages, but also by higher order harmonic voltages such as 5th, 7th, and so on. In practice, the magnitude of these higher order harmonic voltages may be larger than that of the third order harmonic content, as shown in Chapter 3. The influence of higher order harmonic voltages can not be neglected. Although the probe does pick up the 5th, 7th and other harmonic voltages, they can not be compensated for using the technique proposed in [3].

Another error in this method lies in the introduction of the constant ratio of the two factors, k_1 and k_3, as mentioned in 1.2.3.1. However, this error can be eliminated if a user resorts to a real 3-D electric field analysis for every real configuration of MOSA. The 3-D electric field analysis exceeds the scope of the investigation of this project. In order to verify whether or not the measured results are influenced by probe position, tests were conducted using a three-phase configuration in which the probe position was varied; these tests and results are reported in chapter 3.

1.2.4. Neutral Current Method [4, 7]

1.2.4.1. The Principle of Neutral Current Method

As shown in Fig.1.7, the zero sequence leakage current of MOSA, I_0, can be obtained from the neutral line using a shunt or a suitable clamp type CT. If the MOSA in three phases are identical and three-phase voltage is pure sinusoidal voltage and balanced, the sum of the positive and negative components of the leakage current will be zero, and the neutral current I_0 equals to $3I_{r3}$.

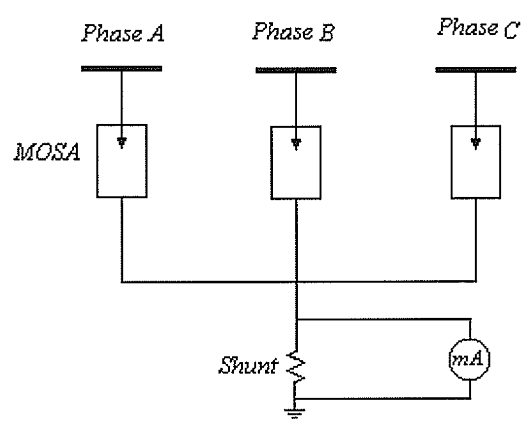

Fig.1.7. Schematic diagram of Neutral Current Method

1.2.4.2. Errors with Neutral Current Method

First, the errors will be caused by unbalanced three-phase voltage. Unbalance of the three phase voltages will result in quite misleading results, even with identical MOSA in three phases. In this case, the sum of positive and negative components will not be zero. The non-zero sum will add to the zero sequence components, and an unacceptable neutral current will be displayed by the milliampere meter, even if the MOSAs are unaged.

If the ageing of the MOSA in the three phases are not identical, as will be discussed in Chapter 3, the extra sum from the negative and positive leakage current components will result in quite confusing results.

The harmonic voltages will also greatly influence the test result. Due to the non-linear characteristics of MOSA valve elements, not only will the fundamental component of the applied voltage result in the 3^{rd} harmonic resistive leakage current, but also the 3^{rd}, 5^{th}, 7^{th}, etc. Besides, the 3^{rd} harmonic voltage components will result in $3I_{c3}$, which will add up to the neutral current. This will result in a much greater reading in the milliampere meter. This aspect is more fully discussed in Chapter 2.

Besides, non-pulsating leakage current due to the lowered surface resistance of the housing will influence the reading of the milliampere meter. Furthermore, if the MOSA in the three phases age identically, this method can not distinguish whether the increased current is due to MOSA ageing or due to external effects.

Thus, in order to make full use of the advantage of this method, modifications need to be introduced and the testing technique needs to be improved. The suggested modifications of this method are discussed in Chapter 3.

1.3. Scope of Present Investigation

For the currently used techniques mentioned above, the influence of voltage harmonics on the resistive leakage current and its 3^{rd} harmonic component of MOSA are studied first. The results of the diagnostic testing techniques obtained by using a laboratory set-up are reported. Finally, the validity of the simple representation model of MOSA is discussed.

1.3.1. Study of the Influence of Harmonic Voltage on On-site Testing of MOSA

In this study, the representation of v-i_r characteristics of MOSA in the low electric field region is first discussed. The harmonic components of resistive leakage current of aged and unaged MOSA under pure sinusoidal voltage are simulated. The effects of non-sinusoidal voltage on the harmonic component of the leakage resistive current are then studied. Finally, the results of the resistive leakage current under non-sinusoidal voltage are compared with those from the aged MOSA under pure sinusoidal voltage.

1.3.2. Investigation of the Techniques for On-site Diagnostic Testing of MOSA

(1). First, the v-i_r characteristics of some aged and unaged MOSA are derived experimentally.

(2). Secondly, three kinds on-site diagnostic testing techniques are investigated; i.e. investigation of the resistive leakage current method, probe method and the neutral current method. The test results of each technique are discussed and analysed. Possible improvements are suggested for the resistive leakage current and the neutral current methods.

1.3.3. Brief Discussion of the Simple Representative Model of MOSA

The test results show that the present practice of using a simple representation of MOSA, which consists of a constant capacitor and a non-linear resistor in parallel is questionable. This aspect is discussed briefly in Chapter 3.

CHAPTER 2

Influence of Voltage Harmonics on MOSA Resistive Current Used as a Diagnostic Indicator

As mentioned in Chapter 1, in order to ascertain the condition of a MOSA many on-site methods have been suggested of which leakage current based methods are the most popular. These methods utilize the resistive portion of the leakage current which is non-sinusoidal because of the non-linear volt-ampere characteristics of the MOSA. Either the magnitude of the resistive current or its harmonic component, notably the third order component, may be used as a diagnostic indicator on a long-time basis. In either case, the total current has to be measured.

Consider the case where the applied voltage is a pure sinusoid i.e., $V=\sqrt{2}\,V_1\cos(\omega t)$. In this case, the measured current, i_t, may be resolved into its resistive and capacitive components i_r and i_c. The component i_r is resolved into its spectral components of which the third harmonic i_{r3} is used as an indicator. The current i_c is of fundamental frequency only, i.e. $i_c = i_{c1}$. It should be noted that i_{r3} exists because of the nonlinear characteristics of the MOSA.

Suppose the applied voltage contains a third harmonic component V_3. In this case

$$v = \sqrt{2}V_1 \cos(\omega t) + \sqrt{2}V_3 \cos(3\omega t + \Phi_3) \qquad (2\text{-}1)$$

The total current,

$$i_t = i_r + i_c \qquad (2\text{-}2)$$

The current i_c consists of fundamental and third harmonic components, i.e.,

$$i_c = i_{c1} + i_{c3} \qquad (2\text{-}3)$$

The component i_{c3} arises due to the presence of the 3rd harmonic in voltage. The current i_r is also composed of fundamental and harmonics. Neglecting all harmonics of order greater than 3.

$$i_r = i_{r1} + i_{r3} + i'_{r3} \qquad (2\text{-}4)$$

In Eq.2-4, i_{r3} arises due to the non-linearity of MOSA volt-amp characteristics whereas i'_{r3} arises due to the presence of the third harmonic in voltage,

V_3. The magnitude of i'_{r3} depends on the magnitude of V_3 and its phase angle Φ_3. The above suggests that it is not only necessary to account for i_{r3} as has been done in [3] but also to take into effect the influence of i'_{r3}. This aspect has been explored in this chapter.

2.1. Representation of MOSA v-i_r Characteristics in the Low Electric Field Region

2.1.1. Exponential Representation

An exponential representation of the type

$$i_r = cv^{\alpha} \qquad (2\text{-}5)$$

has been proposed in literature [8] which is similar to that used to characterize the behavior of a SiC arrester [10]. In equation (2-5), i_r is the instantaneous value of resistive current and v is the instantaneous value of the phase-ground voltage acting across the MOSA. The constant C is material dependent and α is the rate of change of $\ln(i_r)$ with respect to $\ln(v)$, which is a function of temperature and voltage, $\alpha=\alpha(v, T)$.

Figure 2.1 shows the experimentally obtained v-i_r [9] characteristics pertaining to a new unaged arrester rated at 120kV(V_N=120kV) at a temperature of 20°C; the points denoted by "x" represent experimental data. The best fit to the experimental data of Eq.2.1 obtained by use of the Least-Square-Technique is described by:

$$i_r = 0.096135v^{6.6088}(mA) \qquad (2\text{-}6)$$

which is shown in Fig. 2.1 by the solid line. In Eq.2-6, v is in p.u (p.u. v= actual voltage/arrester rated voltage). From Figure 2.1, it is apparent that the exponential representation is not very accurate. The reason for this can be explained as follows. From equation (2-5), α can be expressed as:

$$\alpha = {d(\ln(i_r))} \Big/ {d(\ln(v))} \tag{2-7}$$

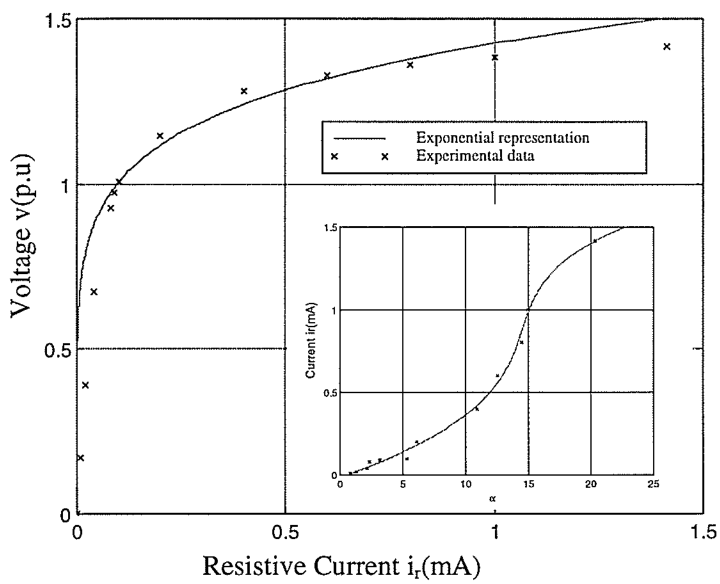

Figure 2.1. 120kV MOSA voltage v– resistive current i_r relation

xxx: experimental data

---: exponential representation according to Eq. 2.1

Inset: α - i_r relation in low electric field region

As shown in the inset of Fig. 2.1, the value of α, for a fixed temperature, changes with i_r, varying from about 0.5 at low i_r to about 20 at a high value of i_r. Use of a constant α value therefore results in considerable error. Eq. 2-5 with constant α value can only be used to represent MOSA v-i_r characteristics in the medium electric field region where α value is relatively constant [8].

2.1.2. Polynomial Representation

As pointed out above, simulation of MOSA behavior in the low electric field region using an exponential representation results in serious error. In order to achieve an accurate fit, a multi-segment polynomial representation is proposed as follows.

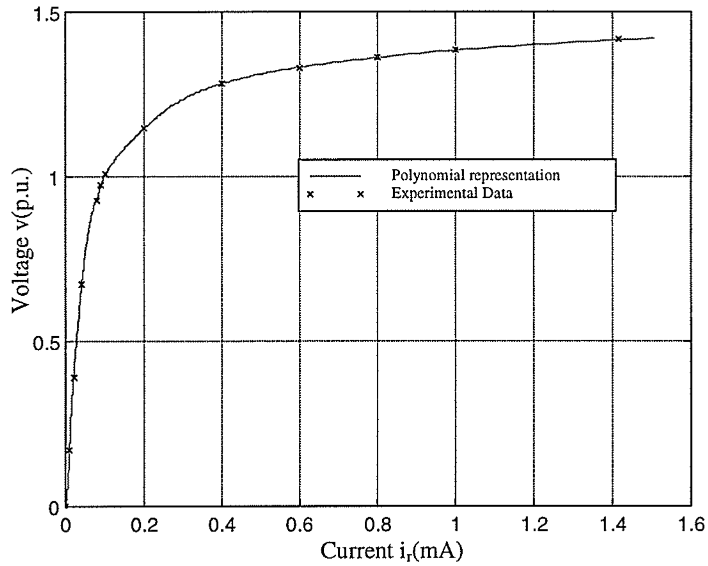

Figure 2.2: 120KV MOSA voltage v – resistive current i_r relation

xxx: experimental data

---: Polynomial representation according to Eqs.2-8 and 2-9

From examination of the data in Figure 2.1, it is obvious that the v-i_r relationship is markedly nonlinear for $v \geq$ 0.8p.u. For $v \leq$ 0.8p.u the nonlinearity, although evident, is not as pronounced. A two segment polynomial representation is therefore proposed. It was found that a good fit could be achieved by using a fifth order polynomial representation. In the voltage range 0-0.8p.u, the polynomial representation is given by:

$$i_r = 0.8765v^5 - 1.9491v^4 + 1.6014v^3 - 0.5401v^2 + 0.1130v \qquad (2\text{-}8)$$

and for voltage greater than 0.8p.u, the representation is:

$$i_r = 208.2v^5 - 1107.8v^4 + 2347.2v^3 - 2476v^2 + 1300.3v - 271.9 \qquad (2\text{-}9)$$

The polynomial representation and the original experimental data are shown in Fig. 2.2. Comparison of Figs.2.1 and 2.2 shows that the polynomial representation is more accurate than the exponential representation.

2.2. Harmonic Components of Resistive Current of Aged and Unaged MOSA under Pure Sinusoidal Voltage

2.2.1. Case 1: Unaged MOSA, Pure Sinusoidal Applied Voltage

In this case, the ac voltage across the unaged arrester is assumed to be a pure sinusoid of the following form:

$$v(t) = \sqrt{2}V\sin(\omega t) \qquad (2\text{-}10)$$

In equation (2-10), $v(t)$ is the instantaneous operating voltage at time t; V is the MCOV (RMS) value, which is about 0.6-0.8 of the reference voltage, V_{ref}, of MOSA. According to the ANSI/IEEE Standard, the reference voltage, which is situated near the knee point of the v-i_r characteristic curve, is almost equal to the rated voltage V_N of most high-voltage arresters. Therefore, the MCOV value lies in the range of 0.6-0.8V_N. In the following, the MCOV is defined to be equal to 0.8V_N.

When the sine wave of period $T\,(T = 1/60 = 0.01667'')$ in Eq.2-10 is discretized with 256 points, i.e. N=256, the discretization interval, τ, is equal to $T/256$. The discrete representation of Eq.2-10 is:

$$v(k) = \sqrt{2}V\sin(k\omega\tau), k = 0,1,2,\ldots,N-1 \qquad (2\text{-}11)$$

For every value of v(k), the corresponding i_r(k) can be calculated from Eqs.2-8 and 2-9. The magnitude spectrum of the harmonic components in i_r can be calculated easily by employing the FFT algorithm.

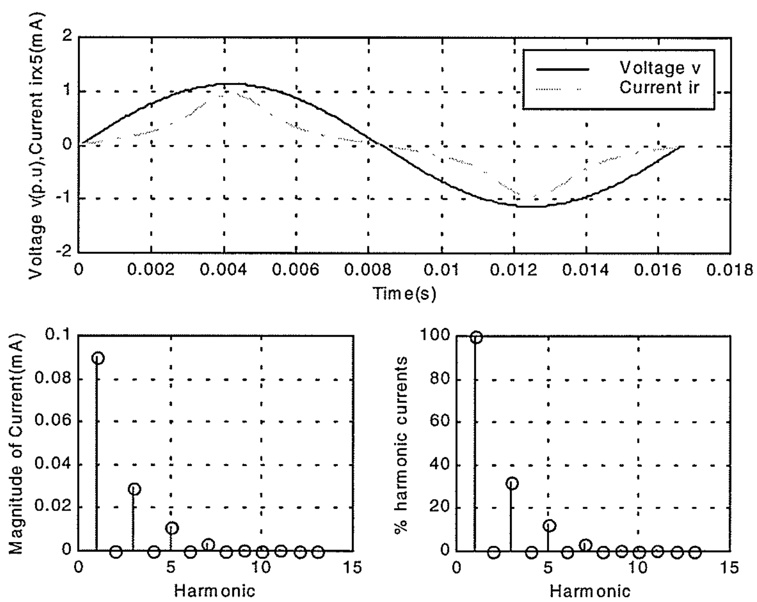

Figure 2.3: Spectrum of resistive harmonic current in unaged 120kV MOSA for pure sinusoidal applied voltage of 96kV(RMS)(Eq. 2-10)

The waveform of applied voltage and resistive leakage current and the corresponding magnitude spectrum of resistive harmonic current are shown in Fig 2.3.

It is obvious that the resistive current $i_r(t)$ is non-sinusoidal. For the arrester under consideration, the RMS value of the resistive current, I_r, is 95.3μA.The RMS value of the fundamental, I_{r1}, and 3rd harmonic component, I_{r3}, are 88.9μA, 31.8μA respectively. The 3rd harmonic content amounts up to 35.78% of the fundamental component. It is seen that, even with a pure sinusoidal voltage acting across an unaged MOSA, the resistive current is not sinusoidal which results in the presence of a 3rd harmonic current.

2.2.2. Case 2: Aged MOSA, Pure Sinusoidal Applied Voltage

For reasons mentioned in Chapter 1, a MOSA ages with time in service. Due to ageing, the magnitude of resistive leakage current increases with resulting increase in harmonic components. The v-i_r characteristics of an aged and unaged MOSA are shown in Fig.2.4. For the aged MOSA, the voltage required to cause 1mA peak resistive current is taken to be 90% or less of the value of the unaged MOSA.

In practice, under this condition, the MOSA is normally removed from service.

For the aged MOSA, the waveform of applied voltage and resistive leakage current and the corresponding magnitude spectrum of resistive harmonic current are shown in Fig 2.5.

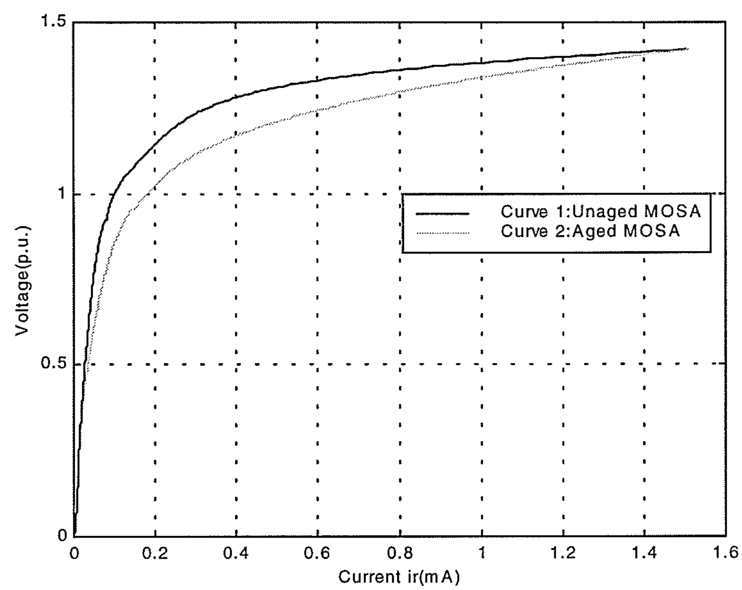

Figure 2.4. v-i_r characteristics of aged and unaged MOSA

From Figs 2.3 and 2.5, the resistive leakage current of a MOSA increases considerably due to ageing. For the aged arrester, at its MCOV, I_r increases to 163.8 μA, which is almost 1.7 times of those obtained under the unaged condition. The 3rd harmonic component I_{r3} is now 56.8μA, which is almost 1.8 times the unaged value. Monitoring the total resistive current or the third order harmonic current enables one to find out the operational condition of MOSA.

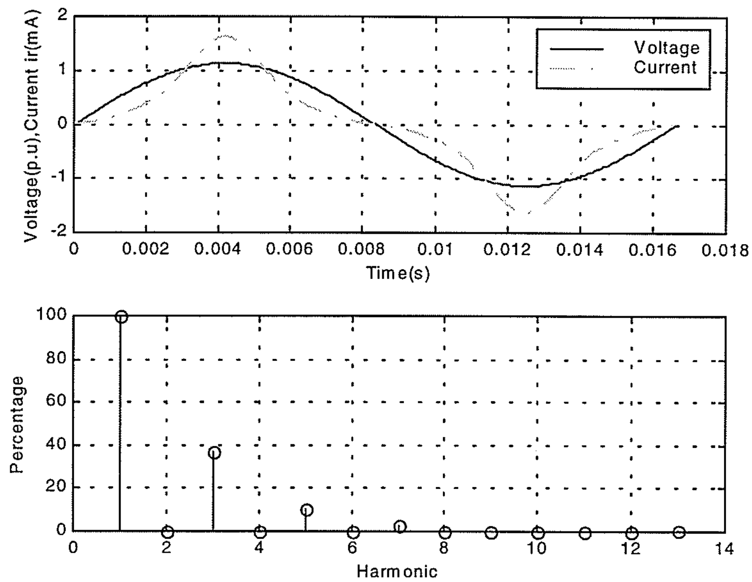

Figure 2.5: Spectrum of resistive harmonic current in an aged 120kV MOSA for pure sinusoidal applied voltage of 96kV(RMS)(Eq.2-10)

2.3. Harmonic Content of Voltage in Power Systems [11]

In a power system, harmonic components are present in the voltage due to many reasons. Harmonic voltages are introduced at the generation end and in transmission and distribution systems due to unbalanced faults, non-linear excitation of power transformers, and increased use of power electronic technology. Even the synchronous generator itself injects harmonic voltage components into a power system. At the customer end, the use of arc furnaces in the iron-steel industry, TV sets, fluorescent lighting installations and the increasing use of Pulse Width Modulation (PWM) drives for ac motors, etc, are very common. All these loads will result

in the injection of harmonic current into the power system and will result in the further distortion of the voltage of the bus at which such loads are connected.

The spread of harmonic currents in power system depends on the power system configuration and results in a very complicated harmonic voltage distribution pattern. Because of the harmonic power flow the harmonic components and content will be rather different in different portions of the same power system i.e. low voltage, medium voltage system, etc. Furthermore, the harmonic contents and their magnitude in a power system will vary with time. The same can be said for the phase angles of the harmonic components. Therefore, in practice, the voltage across a MOSA will never be a pure sinusoid. The harmonic distortion will affect the wave shape and magnitude of the resistive leakage current, which in turn affects the harmonic spectral components. This aspect is investigated in Section 2.4.

2.4. Effect of Nonsinusoidal Voltage on Harmonic Components of the Resistive Current of the unaged 120kV MOSA

As discussed above, the harmonic components in the voltage will never be constant. In the following, the effects of the 3rd and the 5th harmonic components acting alone and in various combinations are discussed.

2.4.1. Effects of 3rd Harmonic in Voltage on the 3rd Harmonic Component of Resistive Leakage Current

In the following, the magnitude of the 3rd harmonic voltage component and its phase angle are designated by V_3 and Φ_3 respectively. The actual voltage across the MOSA is obtained by addition of the fundamental and the 3rd harmonic voltage, components i.e.,

$$v = V_1 \cos(wt) + V_3 \cos(3wt + \Phi_3). \qquad (2\text{-}12)$$

Case1: Φ_3=0°, V_3=3%V_1

The resulting voltage waveform, v, was discretized and the resistive leakage current i_r calculated from the polynomial representation Eqs.2.8 and 2.9. Next, the FFT was performed on the discretized current waveform and the spectral components obtained. The waveform of applied voltage and resistive leakage current and the corresponding magnitude spectrum of resistive harmonic current are shown in Fig. 2.6. Comparison with the results obtained from the unaged MOSA under pure sinusoidal voltage (Fig. 2.3) shows that Ir decreases to 86.6μA, its fundamental component I_{r1} is 82.6μA, and its 3rd harmonic component I_{r3} is 24.5μA which is 29.66% of the fundamental component I_{r1}.

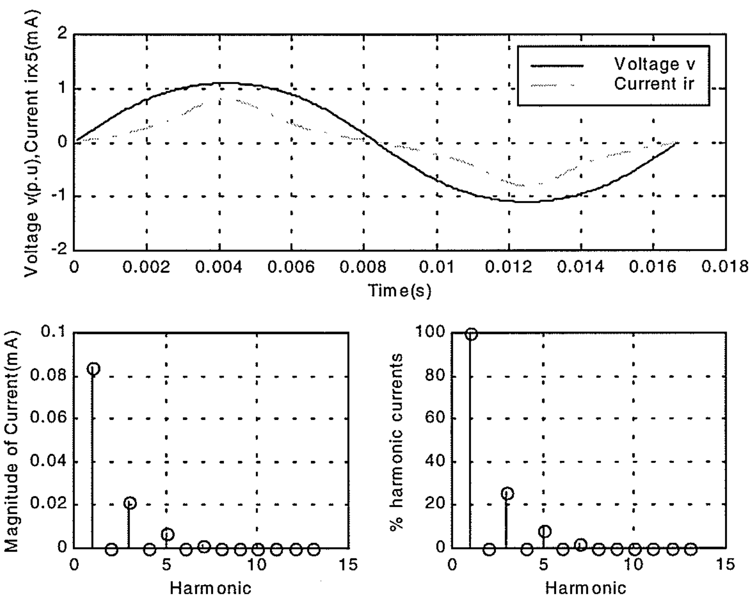

Figure2.6. Spectrum of resistive harmonic current in unaged 120kV MOSA for applied voltage of 96kV(RMS) contaminated with 3% of 3rd harmonic voltage, Φ_3=0° (Eq.2-12)

Case 2: Φ_3=180°, V_3=3%V_1

The waveform of applied voltage and resistive leakage current and the corresponding magnitude spectrum of resistive harmonic current are shown in Fig 2.7.

For this case, I_r =105.1μA, I_{r1}=95.8μA and I_{r3}=39.4μA (41.13% of I_{r1}). Also, as shown in Fig. 2.7, the peak value of i_r is approximately 250μA, compared with 125μA obtained under a pure sinusoidal voltage. This increase can be explained by the increase in the peak value of the voltage when the fundamental component V_1 is added to the triple frequency component V_3 with phase shift Φ_3=180°.

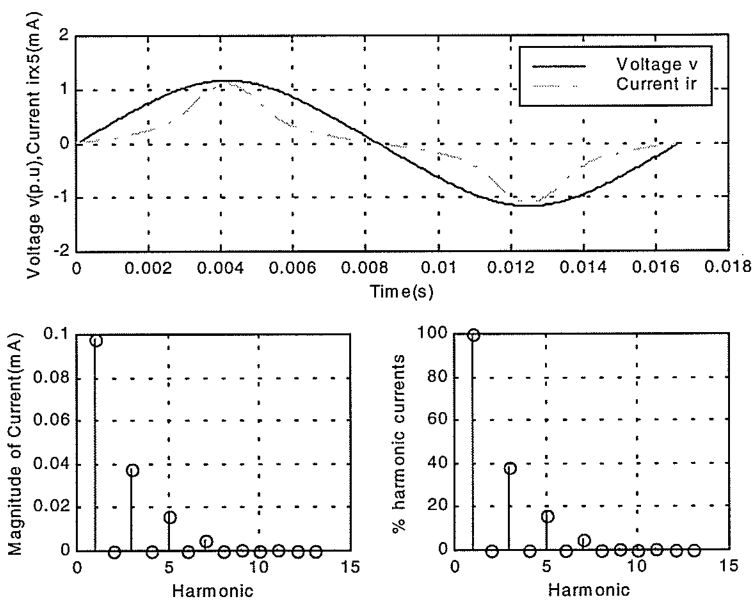

Figure 2.7. Spectrum of resistive harmonic current in unaged 120kV MOSA for applied voltage of 96kV(RMS) contaminated with 3% of 3rd harmonic voltage, Φ_3=180° (Eq.2-12)

Figure 2.8 shows the variation in the percent content of the resistive 3rd harmonic leakage current I_{r3} as a function of the magnitude and phase angle of 3rd harmonic component in the applied voltage.

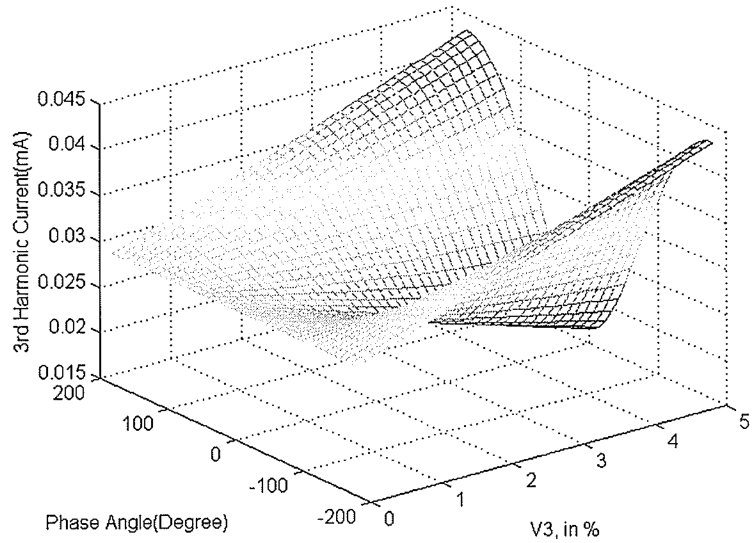

Figure 2.8. Showing dependence of resistive 3rd harmonic current on 3rd harmonic voltage, V_3, and its phase angle, Φ_3 (Eq.2-12)

2.4.2 Effect of 5th Harmonic Voltage on Spectral Components of the Resistive Leakage Current

When only the fifth harmonic is assumed to be present in the voltage, the voltage waveform is described:

$$v = V_1 \cos(wt) + V_5 \cos(5wt + \Phi_5). \quad (2\text{-}13)$$

Case 1: $\Phi_5 = 0°$ and $V_5 = 2\% V_1$.

The waveform of applied voltage and resistive leakage current and the corresponding magnitude spectrum of resistive harmonic current are shown in Fig 2.9. Comparison with the results obtained from the unaged MOSA under pure sinusoidal voltage Fig.2.3 shows that Ir increases to 98.5μA. I_{r1} is now 90.4μA, and I_{r3} is 34.7μA which is 38.38% of the fundamental component, I_{r1}.

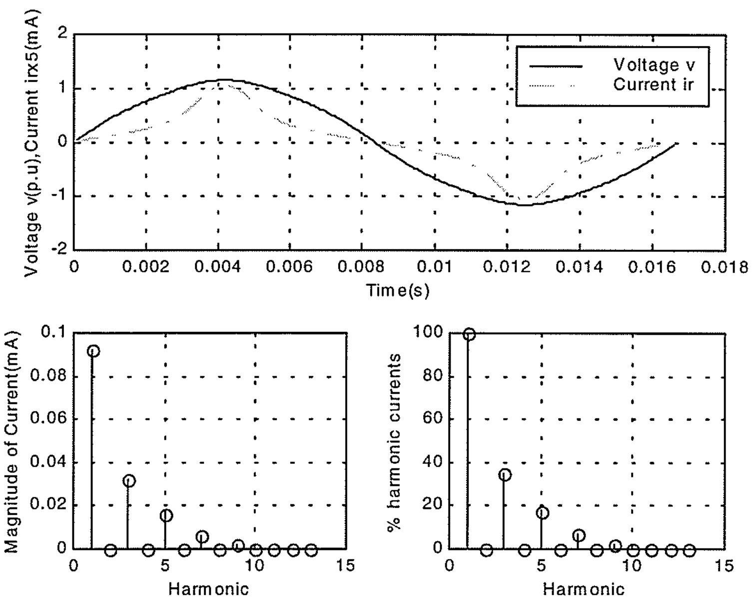

Figure 2.9. Spectrum of resistive harmonic current in unaged 120kV MOSA for applied voltage of 96kV(RMS) contaminated with 2% of 5th harmonic voltage, Φ_5=0° (Eq.2-13)

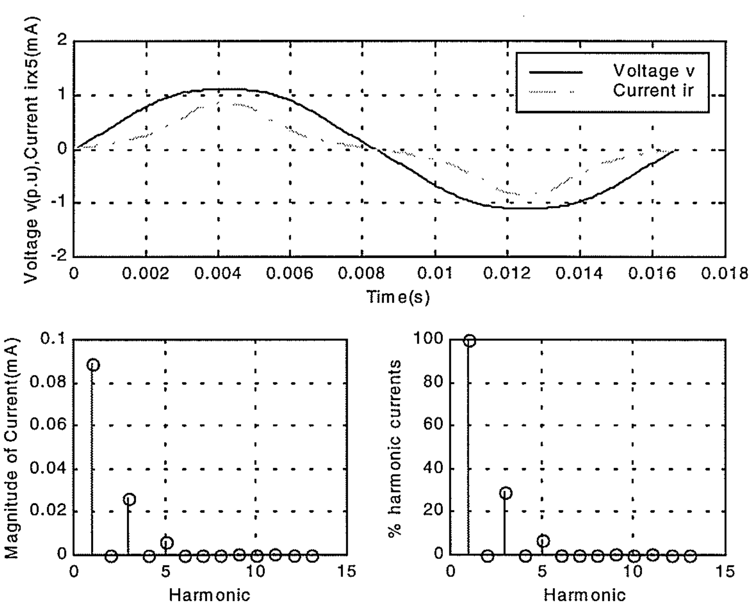

Figure 2.10. Spectrum of resistive harmonic current in unaged 120kV MOSA for applied voltage of 96kV(RMS)contaminated with 2% of 5th harmonic voltage, Φ_5=180° (Eq.2-13)

Case 2: $\Phi_5 = 180°$, $V_5 = 2\% V_1$

The corresponding results are shown in Figure 2.10.

For this case, I_r=92.9μA, I_{r1}=87.9μA and I_{r3}=29.0μA which is 32.99% of the fundamental component, I_{r1}.

Figure 2.11 shows the variation in the percentage content of the resistive 3rd harmonic leakage current I_{r3} as a function of the magnitude and phase angle of 5th harmonic component in the applied voltage.

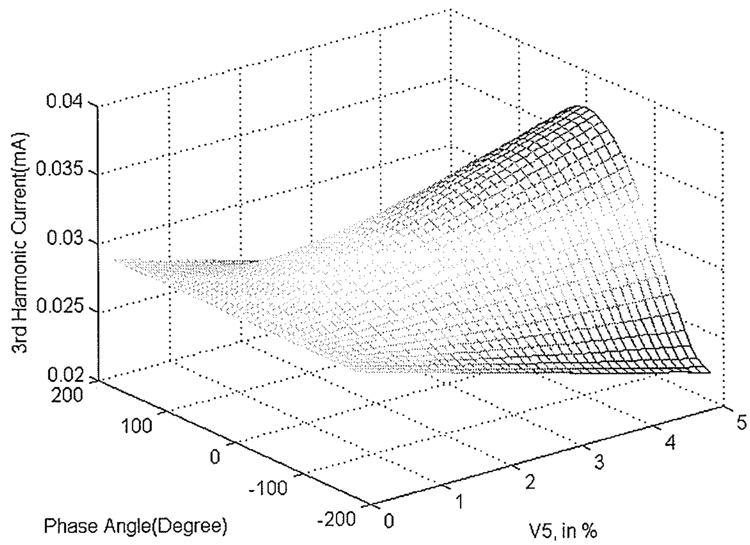

Figure 2.11. Showing dependence of resistive 3rd harmonic current on 5th harmonic voltage, V_5, and its phase angle, Φ_5 (Eq.2-13)

2.4.3. Influence of Combined 3rd and 5th Harmonic Voltage on the 3rd Harmonic Component of the Leakage Current

Five cases are considered as shown in Table 2.1:

The actual voltage across the MOSA is obtained by addition of the fundamental, 3rd and 5th harmonic components, i.e.,

$$v(t) = V_1 \cos(wt) + V_3 \cos(3wt + \Phi_3) + V_5 \cos(5wt + \Phi_5). \qquad (2\text{-}14)$$

Table 2.1: Summary of Simulation Results

Case Number	% of 3^{rd} harmonic voltage	% of 5^{th} harmonic voltage	Phase Angle of V_3 Φ_3 (°)	Phase Angle of V_5 Φ_5 (°)
1	3	2	0	0
2	3	2	0	180
3	3	2	180	0
4	3	2	180	180
5	5	5	180	0

Case 1: $\Phi_3 = 0°, \Phi_5 = 0°$, $\%V_3=3$, $\%V_5=2$

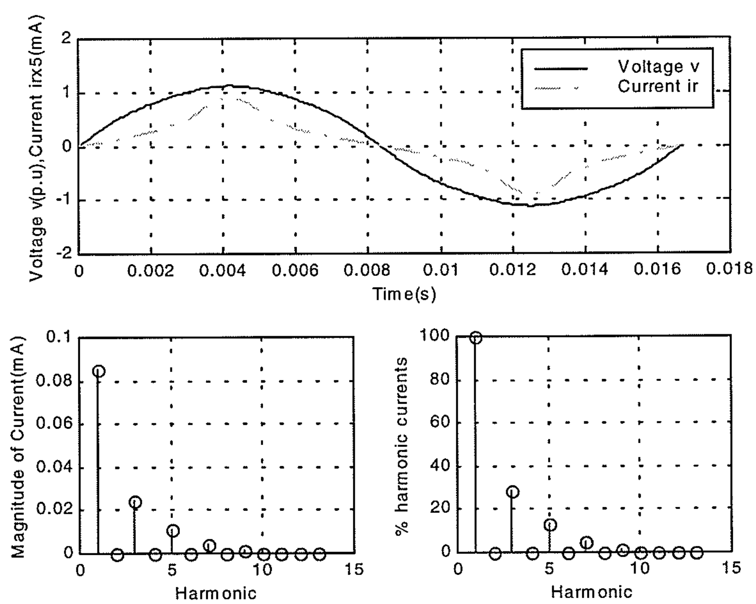

Figure 2.12. Spectrum of resistive harmonic current in unaged 120kV MOSA for applied voltage of 96kV(RMS) contaminated with 3% of 3^{rd} and 2% of 5^{th} harmonic voltage components, Φ_3=0°,Φ_5=0°(Eq.2-14)

The waveform of applied voltage and resistive leakage current and the corresponding magnitude spectrum of resistive harmonic current are shown in Fig

2.12. In this case, I_r=89.2μA, I_{r1} =83.9μA, and I_{r3} =27.3μA (32.54% of the fundamental component).

Case 2: $\Phi_3 = 0^\circ, \Phi_5 = 180^\circ$, $\%V_3$=3 , $\%V_5$=2

The waveform of applied voltage and resistive leakage current and the corresponding magnitude spectrum of resistive harmonic current are shown in Fig 2.13. In this case, I_r=84.8μA, I_{r1} =82.6μA, and I_{r3} =18.8μA (22.76% of the fundamental component).

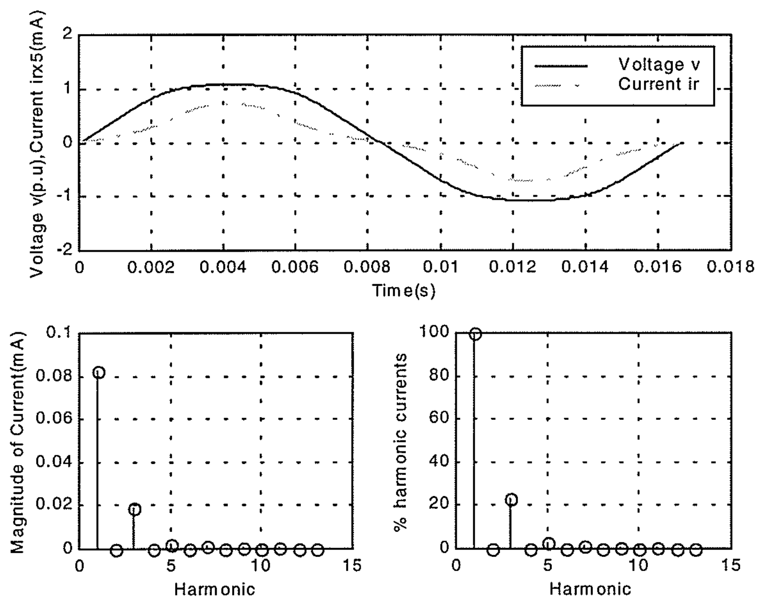

Figure 2.13. Spectrum of resistive harmonic current in unaged 120kV MOSA for applied voltage of 96kV(RMS) contaminated with 3% of 3rd and 2% of 5th harmonic voltage components, Φ_3=0°,Φ_5=180°(Eq.2-14)

Case 3: $\Phi_3 = 180^\circ, \Phi_5 = 0^\circ$, $\%V_3$=3 , $\%V_5$=2

The results are shown Fig 2.14.

In this case, I_r =110.1μA, I_{r1} =99.8μA, and I_{r3} =40.8μA (40.88% of the fundamental component).

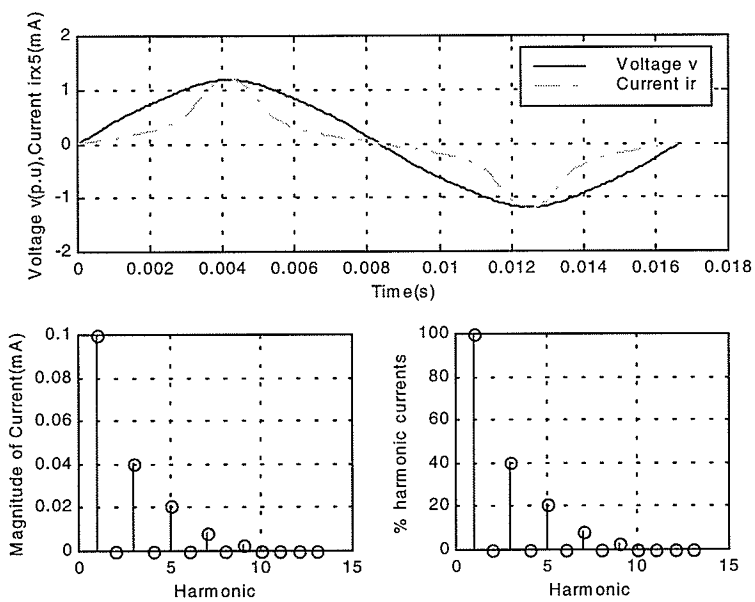

Figure2.14. Spectrum of resistive harmonic current in unaged 120kV MOSA for applied voltage of 96kV(RMS) contaminated with 3% of 3rd and 2% of 5th harmonic voltage components, Φ_3=180°,Φ_5=0°(Eq.2-14)

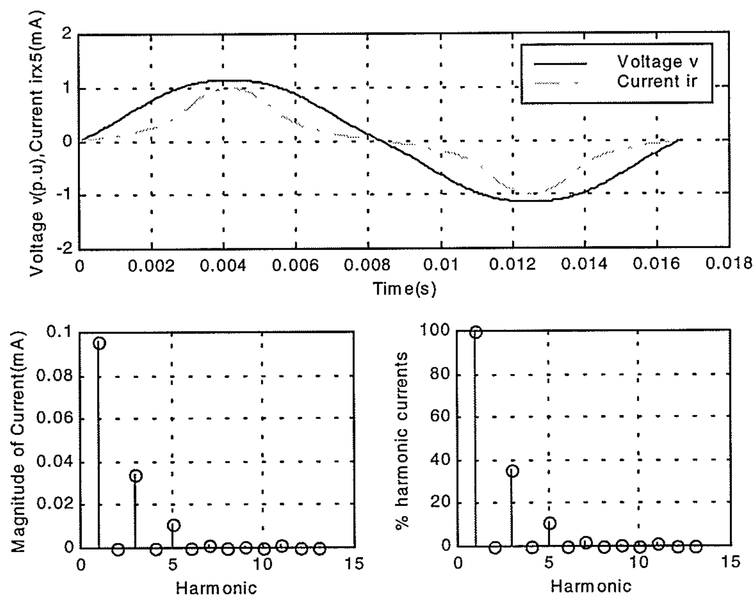

Figure 2.15. Spectrum of resistive harmonic current in unaged 120kV MOSA for applied voltage of 96kV(RMS) contaminated with 3% of 3rd and 2% of 5th harmonic voltage components, Φ_3=180°,Φ_5=180° (Eq.2-14)

Case 4: $\Phi_3 = 180^\circ, \Phi_5 = 180^\circ$, $\%V_3$=3, $\%V_5$=2

The results are shown in Fig 2.15.

In this case, the I_r=102.0μA, I_{r1} =94.5μA, and I_{r3} =36.4μA which is 38.52% of the fundamental component, I_{r1}.

Case 5: $\Phi_3 = 180^\circ, \Phi_5 = 0^\circ$, $\%V_3$=5, $\%V_5$=5

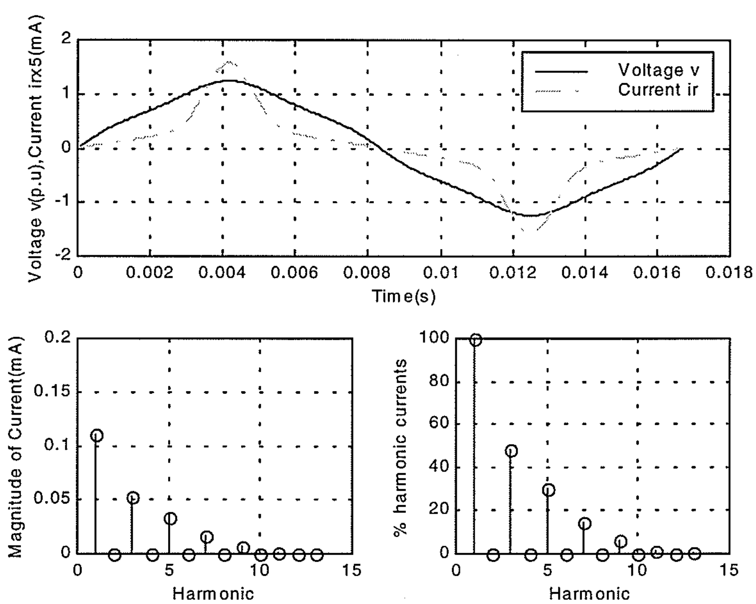

Figure 2.16. Spectrum of resistive harmonic current in unaged 120kV MOSA for applied voltage of 96kV(RMS) contaminated with 5% of 3rd and 5th harmonic voltage components, Φ_3=0°,Φ_5=180°(Eq.2-14)

In this case, the phase angles are the same as that in Case 4 but both the 3rd and 5th harmonic components in voltage are increased to 5%. The waveform of applied voltage and resistive leakage current and the corresponding magnitude spectrum of resistive harmonic current are shown in Fig 2.16.

As shown in Figure 2.16, there is an obvious distortion of the voltage wave shape. For this case I_r=128.8μA, I_{r1}=110.8μA and the I_{r3} increases to 53.6μA.

2.5. Summary of the Simulation Results for Unaged MOSA

A summary of the simulation results for the unaged MOSA is listed in Table 2.2.

Table 2.2: Simulation Results for Unaged MOSA

Harmonic Voltage(%)		Phase Angle(°)		I_{r1} (μA)	I_{r3} (μA)	I_{r3}/I_{r1} (%)	I_{r5} (μA)	I_{r5}/I_{r1} (%)	Ir_{RMS} (μA)
V_3	V_5	Φ_3	Φ_5						
5	5	180	0	110.8	53.6	48.38	33.3	30.05	128.8
3	2	180	180	94.5	36.4	38.52	11.9	12.59	102.0
3	2	180	0	99.8	40.8	40.88	20.8	20.84	110.1
3	2	0	180	82.6	18.8	22.76	2.2	2.66	84.8
3	2	0	0	83.9	27.3	32.54	12.7	15.14	89.2
0	2	-	180	87.9	29.0	32.99	7.6	8.65	92.9
0	2	-	90	89.1	32.0	35.92	13.4	15.04	95.7
0	2	-	0	90.4	34.7	38.38	17.0	18.81	98.5
3	0	180	-	95.8	39.4	41.13	16.9	17.64	105.1
3	0	90	-	89.5	32.7	36.54	13.1	14.64	96.2
3	0	0	-	82.6	24.5	29.66	8.2	9.93	86.6
0	0	-	-	88.9	31.8	35.77	12.4	13.95	95.3

Examination of Table 2.2 shows that the magnitude of I_{r3} depends not only on the harmonic content in voltage, but also on its phase angle.

For example, with only 3% of the 3rd harmonic voltage present, I_{r3} varies in the range of 24.5μA to 39.4μA depending on the value of Φ_3. A similar statement may be made with regard to the 5th harmonic voltage, V_5. When both V_3 and V_5 (content 3% and 2% respectively) are present, the results show that I_{r3} varies in the range of 18.8μA to 36.4μA.

From section 2.2.2, with a pure sinusoidal voltage applied on the aged 120kV MOSA, I_{r3}=56.8μA, and I_r=163.8μA. From Table 2.2, with 5% of 3rd and 5th harmonic voltage present, the maximum value of I_{r3} is 53.6μA(Row 1, Table 2.2) for the unaged MOSA which is almost the same as that obtained for an aged MOSA under pure sinusoidal voltage.

Should the harmonic content in voltage decrease to 3% of 3rd harmonic voltage and 2% of the 5th harmonic voltage, I_{r3} has a maximum value of 40.8μA(Row 3, table 2.2) which is comparable to 53.6μA - the value of I_{r3} obtained with an aged MOSA under purely sinusoidal voltage.

From the above, it is clear that the use of 3rd harmonic of the resistive leakage current as an indicator may result in error if the voltage across the arrester in service is not a pure sinusoid.

Chapter 3

Investigation of On-site Diagnostic Testing Techniques of MOSA

In Chapter 2, the influence of harmonic voltages on the resistive leakage current and its 3rd harmonic component, which are commonly used to indicate the condition of MOSA, has been investigated. In addition to the influence of power system conditions, the limitations of each on-site diagnostic testing method should not be ignored either. In this chapter, the resistive leakage current method, probe method and neutral current method are examined.

3.1. Investigation of the v-i_r Characteristics of MOSA

In order to investigate the on-site diagnostic techniques, it is necessary to use MOSA valve elements with nearly identical v-i_r characteristics. In order to choose the elements, the setup of Fig.3.1 was used.

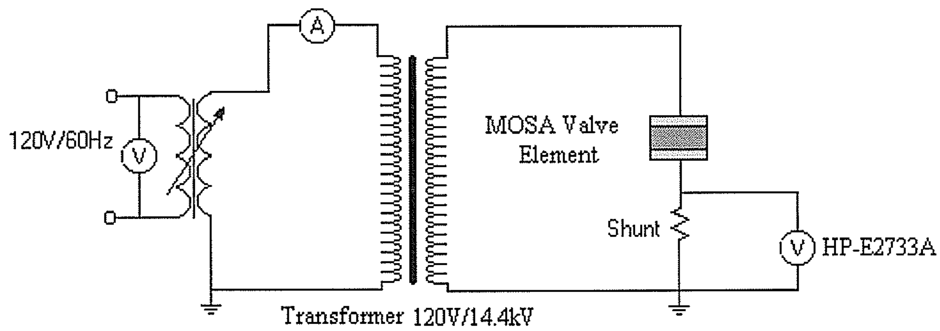

Figure 3.1. Circuit to determine MOSA parameters

In the above test circuit, the shunt is a 10kΩ non-inductive resistor. From a reading of the voltage across this shunt, the RMS value of the total current was determined. The test results are listed in Table 3.1.

From the data in Table 3.1, it is found that MOSA elements #5 and #12 are damaged, #04 and #06 are aged, and #02, #09, #10, #11, #14 and #16 have almost identical V-I characteristics which is shown in Fig.3.2.

The aged MOSA elements were used in the experiment to ascertain the sensitivity of on-site diagnostic methods.

Table 3.1: Test data of MOSA valve elements #1 to #16

		Test #1	Test #2	Test #3	Test #4	Test #5	Test #6	Test #7	Test #8
V.E #1	V(kV)	1.02	1.63	2.06	2.78	3.49	4.49	5.54	6.14
	I(mA)	0.233	0.375	0.461	0.612	0.747	0.937	1.183	1.480
V.E #2	V(kV)	1.01	1.63	2.07	2.78	3.49	4.47	5.59	6.14
	I(mA)	0.218	0.356	0.444	0.581	0.712	0.888	1.108	1.343
V.E #3	V(kV)	1.02	1.66	2.07	2.79	3.49	4.49	5.54	6.14
	I(mA)	0.221	0.365	0.444	0.581	0.712	0.888	1.108	1.343
V.E #4	V(kV)	1.02	1.60	2.08	2.77	3.49	4.57	5.06	6.21
	I(mA)	0.241	0.380	0.485	0.637	0.782	0.992	1.265	1.713
V.E #5	V(kV)	1.01	1.68	2.06	2.71	3.60	4.50	--	--
	I(mA)	0.231	0.394	0.486	0.627	0.977	2.014	--	--
V.E #6	V(kV)	1.01	1.71	2.05	2.77	3.50	4.47	5.54	6.13
	I(mA)	0.231	0.298	0.472	0.631	0.778	0.954	1.279	1.878
V.E #7	V(kV)	1.02	1.73	2.07	2.78	3.52	4.55	5.50	6.11
	I(mA)	0.228	0.388	0.456	0.591	0.753	0.973	1.300	1.723
V.E #8	V(kV)	1.04	1.71	2.08	2.80	3.52	4.54	5.60	6.26
	I(mA)	0.231	0.279	0.458	0.603	0.740	0.932	1.172	1.555
V.E #9	V(kV)	1.02	1.74	2.10	2.80	3.40	4.56	5.60	6.23
	I(mA)	0.224	0.383	0.456	0.602	0.711	0.914	1.148	1.487
V.E #10	V(kV)	1.01	1.69	2.10	2.81	3.52	4.49	5.54	6.22
	I(mA)	0.219	0.367	0.444	0.592	0.730	0.888	1.119	1.368
V.E #11	V(kV)	1.02	1.70	2.10	2.81	3.40	4.60	5.50	6.24
	I(mA)	0.222	0.371	0.454	0.595	0.697	0.909	1.093	1.415
V.E #12	V(kV)	1.01	1.70	2.08	2.74	3.64	4.34	--	--
	I(mA)	0.247	0.420	0.509	0.676	1.076	1.994	--	--
V.E #13	V(kV)	1.01	1.67	2.10	2.76	3.50	4.52	5.53	5.95
	I(mA)	0.183	0.314	0.400	0.528	0.673	0.867	1.092	1.276
V.E #14	V(kV)	1.04	1.69	2.08	2.77	3.54	4.47	5.63	6.24
	I(mA)	0.227	0.372	0.451	0.586	0.730	0.894	1.131	1.412
V.E #15	V(kV)	1.02	1.72	2.07	2.75	3.52	4.52	5.53	6.21
	I(mA)	0.223	0.375	0.450	0.590	0.733	0.923	1.165	1.556
V.E #16	V(kV)	1.03	1.68	2.08	2.79	3.53	4.51	5.65	6.23
	I(mA)	0.226	0.377	0.450	0.592	0.730	0.905	1.143	1.440

V.E: Valve Element, V, I are RMS values

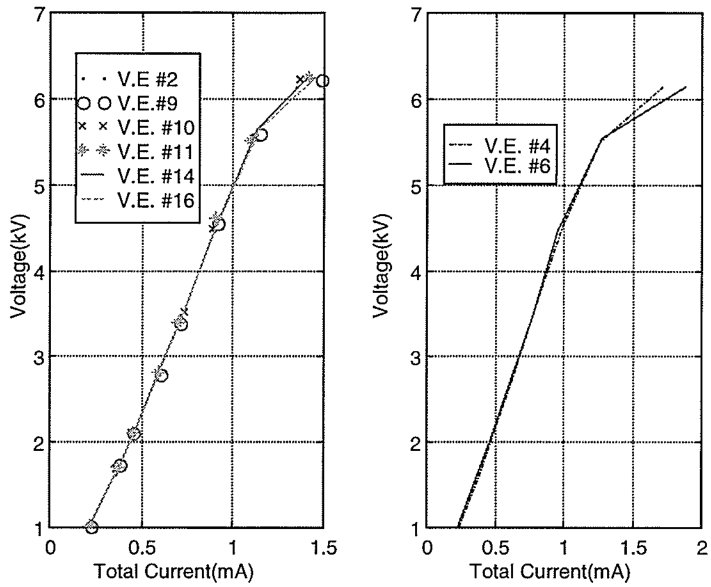

Figure 3.2. V-I Characteristic Curves of the tested MOSA valve elements (V.E: MOSA valve element)

3.2. On-site Diagnostic Test Method Comparison Strategy

This thesis investigates two on-site diagnostic test methods of MOSA, i.e. the neutral current method and the probe method. In order to check the accuracy of these two methods, it is necessary to compare the test results from these two methods with that from a direct method, using a single phase setup. In the direct method, two signals, i.e. v and i, are used to determine the equivalent C of MOSA. With the known C value, I_r and I_{r3} can then be obtained using the compensation technique. Moreover, the single phase setup does not introduce the effects associated with three-phase interference. Thus, the results obtained by use of this method produce a benchmark for comparison with the two on-site diagnostic test techniques considered in this work.

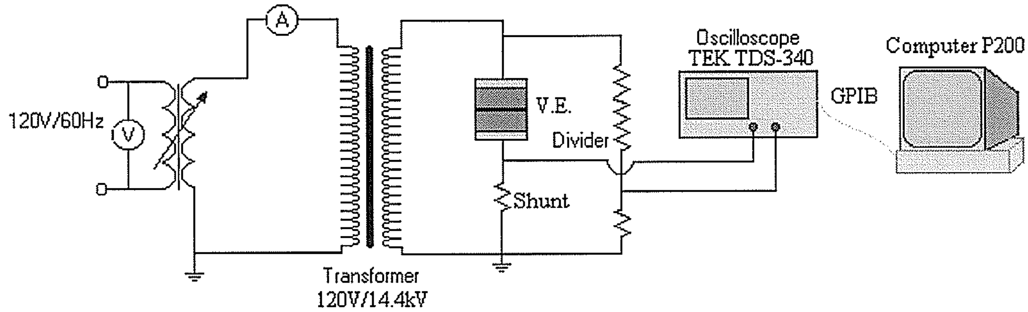

Figure 3.3. Schematic diagram of single phase laboratory set-up to obtain MOSA leakage current (V.E.: MOSA valve element)

Fig.3.3 shows the setup for single phase tests. Two MOSA valve elements in series were used. The shunt is purely resistive with a resistance value of 9.94kΩ. The divider is a purely resistive divider with a ratio of 2500:1 (50MΩ/20kΩ). The total current signal was obtained from the shunt while the voltage was obtained from the divider. These two signals were input into the digital oscilloscope, TEK TDS-340. Through a GPIB interface, the signals were then sent from the oscilloscope to a computer, P200. With the obtained voltage and current signals, the resistive leakage current and its 3^{rd} harmonic component were calculated using the compensation technique discussed in section 3.3.

3.3. Compensation Technique [5, 6, 7]

As shown in Fig.1.2, because $R_z << R_i$, the influence of R_z can be neglected for normal operation. The simplified MOSA representation is shown in Fig.3.4.

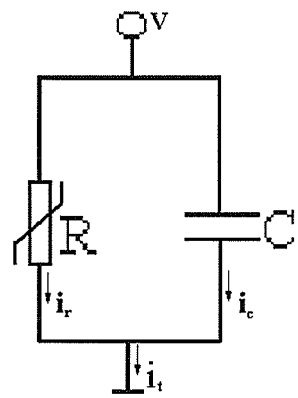

Figure 3.4. Simplified electrical representation of MOSA

As shown in Fig.3.4, $i_t = i_r + i_c$.

If the applied voltage is pure sinusoidal, i.e., $v = v_1$, then $i_c = i_{c1}$. If a suitable k is selected to satisfy

$$i_r = i_t - Gv_{s0} \tag{3-1}$$

where v_{s0} is the voltage v phase shifted forward by 90°, G is a constant which corresponds ωC where C is the capacitance in Fig.3.4, then [95Cha]

$$\int_0^{2\pi} v_{s0}(i_t - Gv_{s0})d(\omega t) = 0 \tag{3-2}$$

In Eqs.3-1 and 3-2, $G = 1000\omega CV_N$

Eq.3-2 can be taken as the criteria for the complete compensation of the capacitive component in a R-C circuit, and the resistive component i_r can be calculated from Eq.3-1.

Applying FFT to the discretized i_r, another indicator i_{r3} may be obtained as well.

Unfortunately, as stated in Chapter 2, the system voltage is seldom a pure sinusoid. Suppose

$$v = \sum_n v_n \tag{3-3}$$

For the capacitive branch of the representation shown in Fig.3.4, the corresponding capacitive current can be written as

$$i_c = \sum_n i_{cn} \tag{3-4}$$

In Eq.3-4, the harmonic components i_{cn} correspond to the same order of harmonic voltage v_n, i.e. $I_{c1} = \omega CV_1$, $I_{c3} = 3\omega CV_3$ and so on. In other words, the magnitude of I_{c3} depends only on V_3.

For the resistive branch, as discussed in Chapter 2, i_{rn}, however, the above is not true. For example, the magnitude of I_{r3} depends not only on V_3 but also on other components. The current i_r is

$$i_r = \sum_n i_{rn} \tag{3-5}$$

In this case the integral in Eq.3-2 does not vanish, i.e.,

$$\int_0^{2\pi} v_{s0}(i_t - Gv_{s0})d(\omega t) \neq 0 \tag{3-6}$$

In contrast with Eq.3.2, in order to compensate for the influence of harmonic voltages, the criteria for pure sinusoidal applied voltage needs to be modified as shown below.

Since

$$\int_0^{2\pi} i_{c1}(i_c - i_{c1})d(\omega t) = 0 \tag{3-7}$$

and

$$\int_0^{2\pi} i_{c1} i_{rn} d(\omega t) = 0, n = 1,2,3,... \tag{3-8}$$

But,

$$\int_0^{2\pi} i_{cn}^2 d(\omega t) \neq 0, n = 1,3,5,... \quad (3\text{-}9)$$

the criteria of Eq.3-2 was modified as follows in the present work.

In Eq.3-1 v_{s0} is replaced with v_{1s0}, the fundamental component of v_{s0}. Next, a suitable G is selected so that

$$\int_0^{2\pi} v_{1s0}(i_t - Gv_{1s0})d(\omega t) = 0 \quad (3\text{-}10)$$

In the above equation, G has the same significance as explained in page 43.

3.3.1. Application of Compensation Technique to Obtain the Capacitance of MOSA Elements; Single Phase System

Fig.3.5 shows the wave-shapes of the applied voltage and leakage current when rated voltage (11kV, RMS) is applied across the series combination of two valve elements, i.e. #10&#14 (Table 3.1).

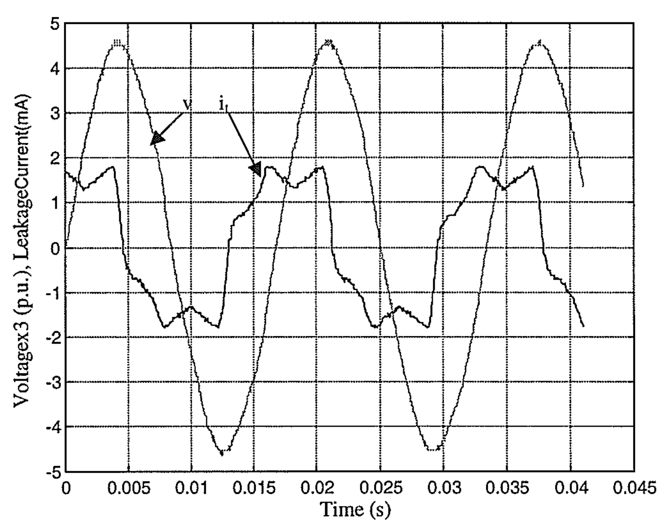

Figure 3.5. Waveshapes of MOSA applied voltage and total current, V.E.#10&#14 in series.

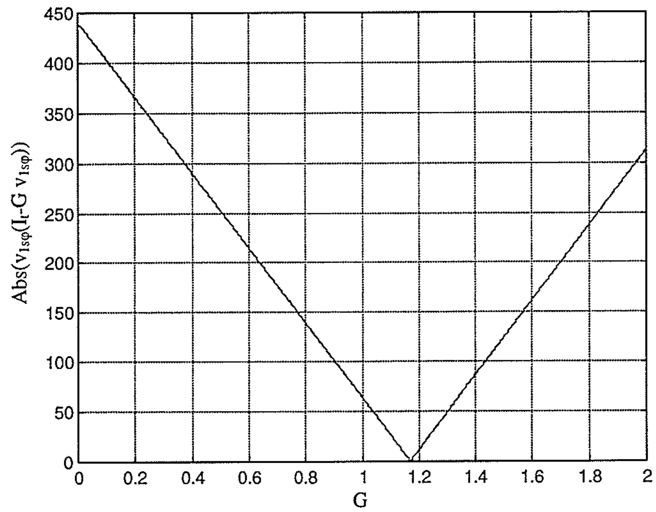

Figure 3.6. Showing calculation for the equivalent C of MOSA set, V.E. #10&#14.

Applying FFT on the discretized voltage signals, the magnitude and phase angle of the fundamental voltage component v_1 can be obtained. Using the modified criteria of Eq.3-10, the value of G may be obtained. As shown in Fig.3.6, G equals 1.160, i.e, the value of C of the MOSA set (#10 and #14) is 279 pF.

3.3.2. Diagnostic Indicator Obtained from Direct Method on a One-phase System; Benchmark Method

After obtaining C, from the known magnitude and phase angle harmonic voltages, the resistive leakage current can be calculated as:

$$i_r = i_t - \sum_n n\omega C v_{n0}, n = 1,2,3,... \qquad (3\text{-}11)$$

In Eq.3-11, v_{n0} is the n^{th} order harmonic voltage phase shifted forward by 90°.

The wave-shapes of applied voltage, capacitive current and resistive current are shown in Fig.3.7.

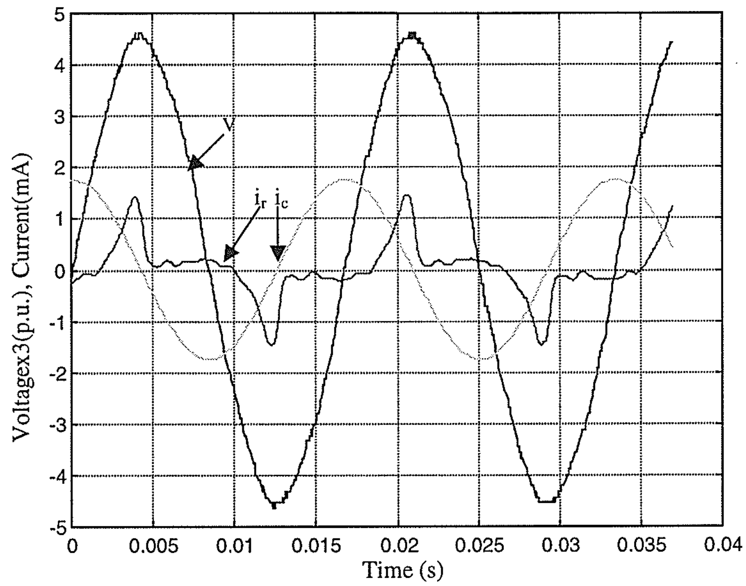

Figure 3.7. Showing the waveshapes of applied voltage, capacitive and resistive leakage currents of MOSA(V.E. #10&#14)

The spectrum of applied voltage and leakage current are shown in Fig.3.8. The THD, total harmonic distortion, of the test voltage is 2.50%; V_3/V_1=0.32%, V_5/V_1=2.07% and V_7/V_1=0.27%. The magnitude of I_r is 0.5283 mA and that of I_{r3} is 0.2810mA.

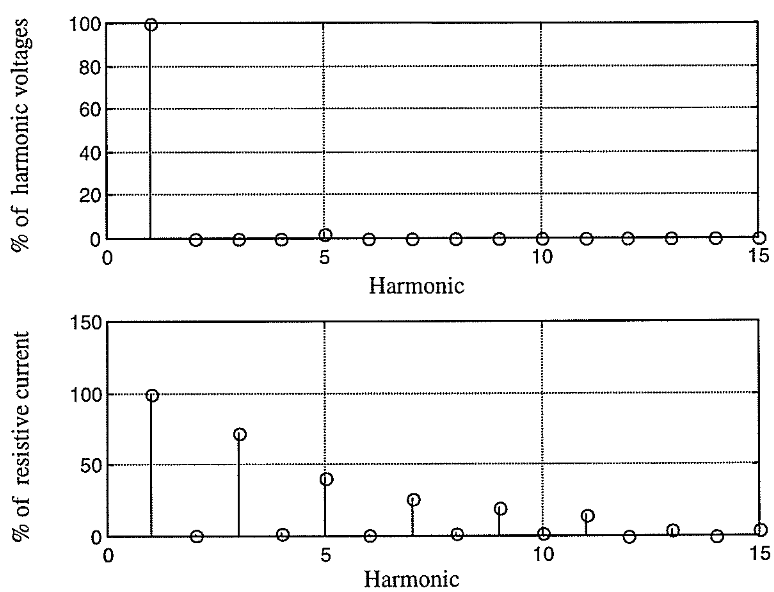

Figure 3.8. Spectrum of the applied voltage and i_r

Similarly, the i_r curves and FFT analysis results of the aged MOSA set #04&#06 and other MOSA sets were obtained. The total resistive leakage currents and the 3rd harmonic component of the resistive leakage currents of the MOSA sets consider are shown in Table 3.2.

Table.3.2. I_r and I_{r3} of MOSA sets

MOSA / Current	Unaged set #10&#14	Unaged set #02&#16	Unaged set #09& #11	Aged set #04&#06
I_r(mA)	0.5283	0.5236	0.5116	0.7936
I_{r3}(mA)	0.2810	0.2793	0.2661	0.3940

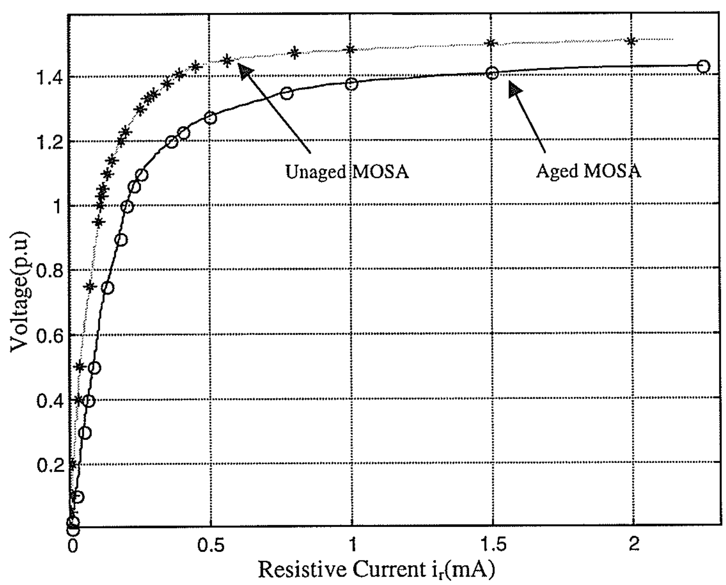

Figure 3.9. Average v-i_r characteristic curves of aged and unaged MOSA sets

From the above, v_l and i_r for each MOSA set is known. Their waveshapes are also known. Therefore, it is possible to plot v_l-i_r curve. The characteristic curve thus obtained was found to be non-single valued and displayed characteristics of hysterisis.

From this v-i_r loop, the average v-i_r characteristics curve was obtained by locating the mid points of the loop. Such characteristics are shown in Fig.3.9 for the unaged MOSA sets #10&#14, #02&#16, #09&#11, and the aged MOSA set #04&#06.

3.3.3. MOSA Diagnostics in a Three Phase System Utilizing the compensation Technique

In sections 3.3.1 and 3.3.2, application of the compensation technique to a single phase system has been discussed. As a matter of fact, this method has been widely used for on-site diagnostic tests [5, 7]. However, for reasons mentioned in Chapter 1, the precision of this method has often been questioned.

The most serious problem with this method is the errors which arise due to inter-phase interferences. As mentioned in Chapter 1, for on-site use, a phase shifter is introduced to compensate for the influence of inter-phase coupling. The most difficult problem with the introduction of the phase shifter is to decide the shift angles for each order of harmonic voltage. As we know, the magnitude of harmonic voltages is much smaller than the fundamental component. Thus, the magnitude of the fundamental capacitive current is much greater than that of the harmonic components. Let θ be the angular difference between zero crossings of the leakage currents of the two outer phases. The angle θ can also be taken as the phase angle difference between their fundamental components. For negative sequence components, the phase angles should be shifted by the same magnitude, θ, but in the opposite direction while zero sequence harmonic components, the phase angles do not need shifting. Thus, different sequence harmonic components need different shift angles.

As discussed in Chapter 1, because of interphase interference, the phase angle of phase A current has to be shifted by 3 to 5° forward while the current of phase C has to be shifted backward. If this angle is denoted by θ, the phase angle difference between currents of phases A and C will be $120^{\circ} \pm 2\theta$. If a suitable clamp type CT is applied to phase A, a similar CT can be applied to phase C simultaneously. By checking the phase difference between the peaks of these two signals, it is not difficult to get the value of θ using software.

After determining the value of θ, the magnitude of the shift angle for every order of harmonic voltages can be obtained. A software phase shifter can then be designed. With this software phase shifter, the influence of interphase interferences can then be eliminated.

Another problem with this method is the test errors, which results from voltage harmonics. The capacitive harmonic current components can be totally compensated by the compensation technique introduced above. The resistive current caused by the voltage harmonics, however, is very hard to isolate because of the non-linear and constantly changing characteristics of MOSA. Using the criteria shown in Eq.3-11 together with close monitoring of the system voltage harmonics seems to be the best method to make a correct judgment. With the development of artificial neural network techniques, it may be possible to exclude the influence of harmonic voltages on the resistive leakage current.

With tall arrester columns, the effect of interphase interferences results in uneven voltage magnitude and phase angle distributions along MOSA column in the two outer phases. The need to account for interphase interference becomes very important.

3.3. Investigation of On-site Diagnostic Testing Techniques of MOSA

3.4.1.Principle of the Probe Method [3]

The probe method is also based on a compensation technique. Slightly different from the compensation method above, the probe method directly compensates for the 3rd harmonic capacitive current component in the 3rd harmonic resistive current.

As shown in Fig.3.1, the resistive leakage current can be calculated as:

$$i_r = i_t - i_c$$

For the 3rd harmonic component, I_{r3} can be calculated as:

$$i_{r3} = i_{t3} - i_{c3} \tag{3-12}$$

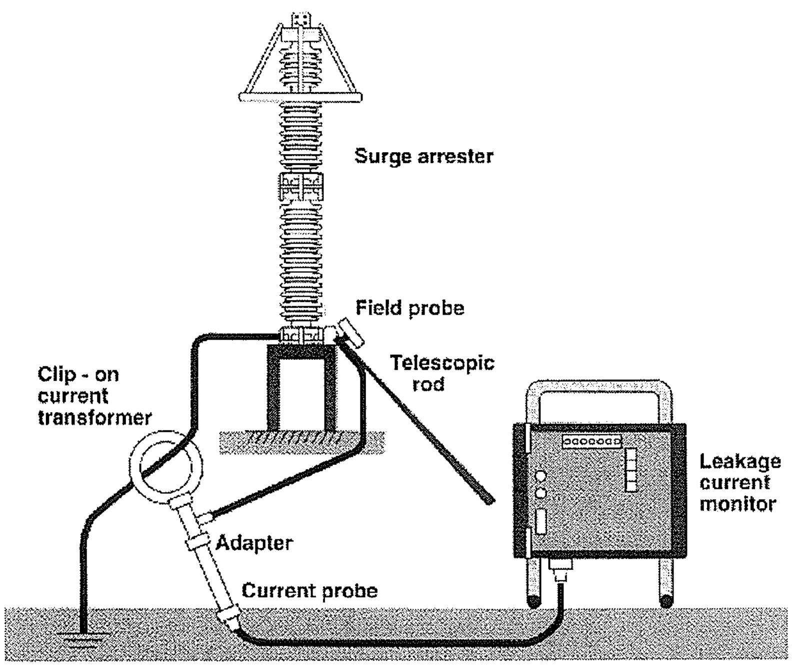

Figure 3.10. Probe Method proposed in [3]

[http://www.transinor.st.no/products/lcm/teclcm.html]

In order to compensate for i_{c3}, a capacitive field probe is introduced as shown in Fig.3.10. The aim of introduction of this probe is to substitute the 3rd harmonic component of the probe current, i_{p3}, with the capacitive current of MOSA, i_{c3}.

Neglecting harmonic voltage components of order >3, the voltage applied across the MOSA can be expressed as:

$$v_n = V_{1n}\cos(\omega t + 2n\pi/3) + V_{3n}\cos(3\omega t + 3n(2\pi/3) + \phi_3) \qquad (3\text{-}13)$$

where n=0,1,2 for three phase, ϕ_3 is the phase angle of 3rd harmonic voltage.

It is known from the above equation that, through pure coupling capacitances between charged three-phase objects and the field probe, the 3rd harmonic components of the probe current i_{p3} should have the same phase angle as i_{c3}.

In order to obtain the 3rd capacitive harmonic current, a scaling procedure for I_{p3} has been introduced by authors in [3]. Since I_{t1} is mostly capacitive, we may write that $I_{t1} \approx I_{c1}$.

Let

$$k_1 = \frac{I_{t1}}{I_{p1}}$$

$$k_3 = \frac{I_{c3}}{I_{p3}}$$

Then

$$I_{c3} = \frac{k_3}{k_1}\frac{I_{t1}I_{p3}}{I_{p1}} \qquad (3\text{-}14)$$

For several typical situations, k_1 and k_3 have been calculated in [3] using a BEM (Boundary Element Method) based computer program. According to the simulation results, the ratio $\frac{k_3}{k_1}$ is thought to be fairly constant and it is claimed that it is therefore possible to apply a single ratio, e.g. 0.75 [3].

Substituting the value of i_{c3} in Eq.3-11 with Eq.3-12, the resistive 3rd harmonic leakage current can now determined from the following equation:

$$i_{r3} = i_{t3} - 0.75\frac{I_{t1}}{I_{p1}}i_{p3} \tag{3-15}$$

3.4.2. Laboratory Setup for Verification of Probe Method

In order to investigate the influence of the position of the probe, a three-phase test circuit (horizontal, flat configuration), shown in Fig.3.11, was setup in the laboratory.

In Fig.3.11, the three 120/14400V, 10kVA distribution transformers were Y/Y connected. Each MOSA column was grounded through a 9.95 kΩ resistive shunt. Each MOSA column comprised of two MOSA valve elements.

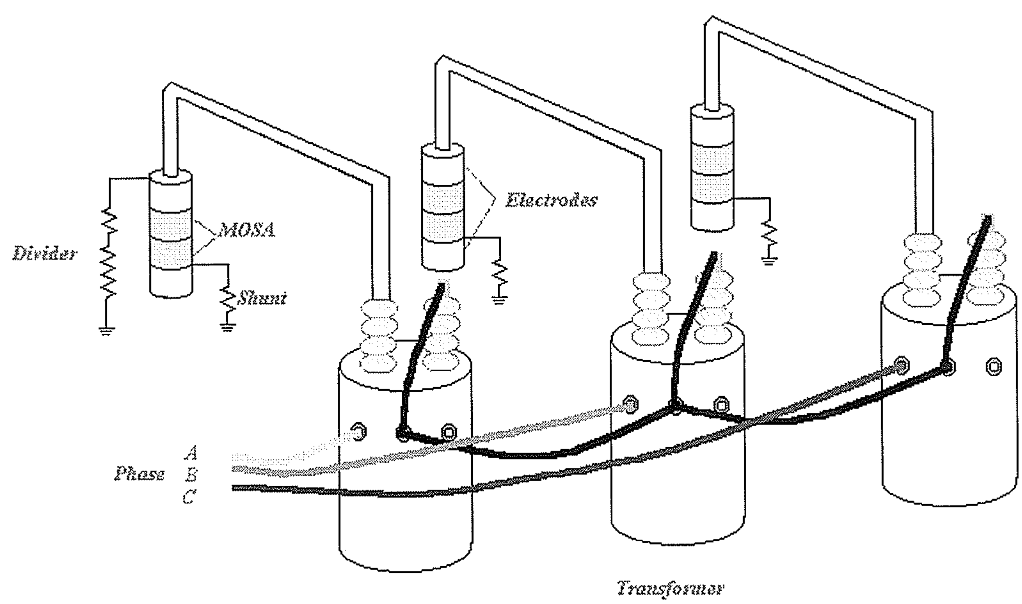

Figure 3.11. Laboratory setup for three-phase test of MOSA

The structure of the capacitive probe and the plate to hold the probe during the test are shown in Fig.3.12. The angles denoted in this figure are the same for all three phases in the test.

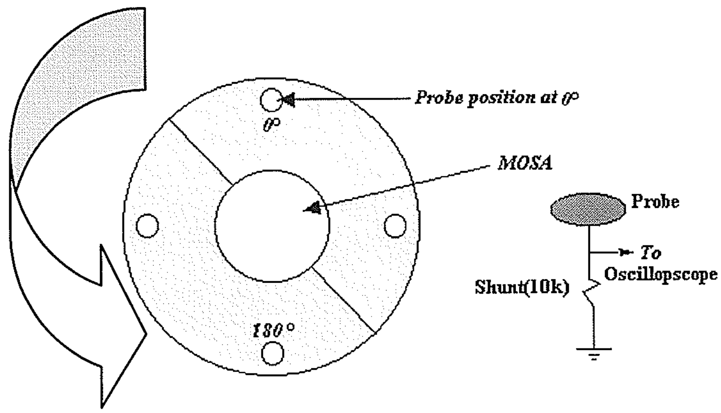

Figure 3.12. Capacitive probe and plate to hold the probe

3.4.3. Comparing Results from Probe Method with the Benchmark Method

With the probe located under phase A, the left most phase, the wave shapes of current i_t and probe current i_p obtained are shown in Fig.3.13. Applying FFT to i_t and i_p, the magnitude and phase angles of I_{1p}, I_{3p} ,I_{1t} and I_{3t} can be obtained. Substituting them into Eq.3-15, the value of i_{r3}, i.e. I_{r3}, can be obtained.

First, the MOSA set, #10&#14, was included in phase A, MOSA sets #02&#16 and #09&#11 were included in phases B and C respectively. The applied voltage was 11kV, and the THD of the applied voltage was 2.48%, V_3/V_1 was 0.01%, V_5/V_1 was 2.10% and V_7/V_1 was 0.13%. The test results are shown in Table 3.3, which includes results by locating the probe at the other three positions.

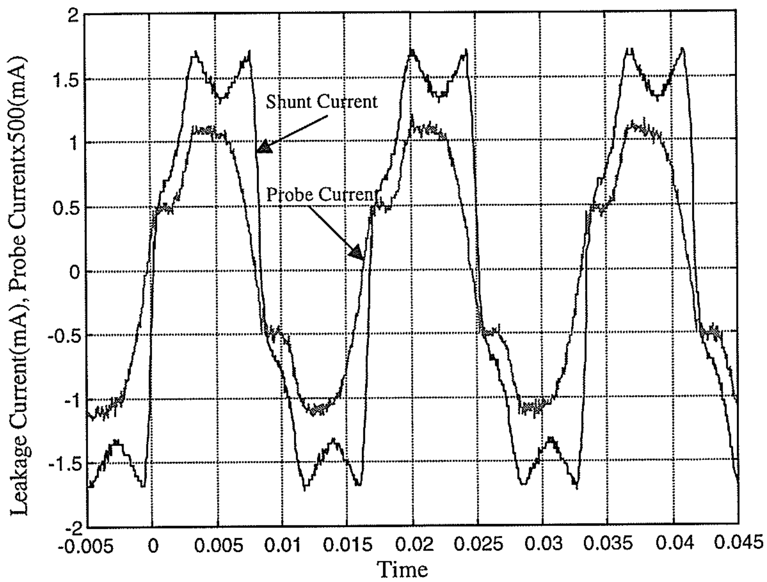

Figure 3.13. Wave shapes of the shunt current and the probe current obtained with the probe located at 0° under phase A (left most phase).

Table.3.3. Test results, probe method

Probe Position / Current		0°	90°	180°	270°
Phase A	I_{r3}(mA)	0.3019	0.2788	0.3079	0.3092
	error(%)	7.44	0.78	9.57	10.04
	Revised k_3/k_1	0.66	0.78	0.44	0.58
Phase B	I_{r3}(mA)	0.3118	0.2807	0.2973	0.2908
	Error(%)	11.64	5.58	6.44	4.12
	Revised k_3/k_1	0.512	0.744	0.66	0.684
Phase C	I_{r3}(mA)	0.2549	0.2773	0.2631	0.2252
	error(%)	4.21	4.21	1.13	15.37
	Revised k_3/k_1	0.88	0.544	0.764	1.16

In Table 3.3, the error (%) in I_{r3} is that obtained by comparison with the benchmark method; the k_3/k_1 is the revised ratio in order to that the I_{r3} value obtained from the probe method is the same as that from the benchmark method.

From Table 3.3, it is found that the magnitude of 3rd harmonic current changes with the position of the probe. For phase A, the minimum I_{r3} occurs at the 90° location, while the maximum value occurs at 270°. The I_{r3} value at 270° is almost 110% of the value at 90°. Comparing with the results from the benchmark method, it is found that the test error with the probe method varies from 0.78% (at 90°) to 10.04% (at 270°); in order to obtain the same result as the benchmark method, the k_3/k_1 ratio should be changed from 0.44 (at 180°) to 0.78 (at 90°). For phase B, the maximum I_{r3} occurs at 0° and is 111% of the value at 90°. For phase C, the maximum I_{r3} is 123% of the minimum value. This shows that test results obtained by the probe method vary with spatial position of the probe.

Comparing with the data obtained from the direct method (section 3.3.2), it is found that the value of I_{r3} in phase A is larger and the value in phase C is obviously smaller.

In order to further verify this, the MOSA sets in phases A and C were interchanged; the test results are shown in Table 3.4.

Table 3.4 shows similar results as in Table 3.3. The results of the 1st and 3rd rows in Table 3.4 should be compared with the results of the 3rd and 1st rows in Table 3.3. This suggests an uneven spatial electric field in a three-phase setup, i.e. a non-constant k_3/k_1 ratio. Thus, the position of the probe will result in errors in on-site diagnostic tests.

Table 3.4. Third harmonic current after interchange of the MOSA columns in phases A and C

Probe Position / Current		0°	90°	180°	270°
PhaseA	I_{r3}(mA)	0.2679	0.2662	0.2466	0.2214
	error(%)	0.67	0.04	7.33	16.80
	Revised k_3/k_1	0.71	0.74	0.88	1.16
PhaseC	I_{r3}(mA)	0.2768	0.2737	0.2691	0.2867
	error(%)	1.49	2.60	4.23	2.02
	Revised k_3/k_1	0.82	0.82	0.88	0.66

3.4.4. Brief Comments on the Probe Method

As discussed in Chapter 2 and in sections 3.4.1-3.4.3, it is found that the probe method can not diagnose the real condition of MOSA due to the influence of harmonic voltages and probe position.

The resistive leakage current, I_r, and it 3rd harmonic component, I_{r3}, are greatly influenced by harmonic voltages. This point has been discussed in detail in Chapter2. As shown in section 3.4.3, the magnitude of the 5th harmonic voltage was around 2% while the 3rd harmonic was around 0.01%. The 5th harmonic voltage dominated in this case while the influence of 3rd harmonic voltage is minor. Using a probe to pick up the 3rd harmonic voltage component and using it to compensate the 3rd harmonic capacitive current [3] will not give out the correct I_{r3} value. Therefore, the probe method will cause quite misleading test results.

As shown in Tables 3.3 and 3.4, for a fixed k_3/k_1 value, if MOSA set #10&#14 was in phase A, the test errors from the probe method, as compared with the benchmark obtained from section 3.3.3, change from 0.78% to 10.04% for different probe position around the MOSA column. Furthermore, in order to obtain the same I_{r3} as the benchmark value, the k_3/k_1 value must be changed from 0.44 to 0.78. This also suggests a rather uneven electric field distribution around the MOSA sets. However, calculation of the electric field distribution before every on-site diagnostic test is not only complex but also unrealistic.

3.5. Neutral Current Method [4, 7]

The principle of this method has been introduced in Chapter 1. In this chapter, test results from several cases will be introduced. The neutral current technique was applied to the following cases using the three-phase laboratory setup of Fig.3.11.

3.5.1. MOSA in All Three Phases Unaged

In this case, the MOSA set #10&#14 (unaged) was inserted in phase A, and MOSA sets #02&#16 and #09&#11(also unaged) were inserted in phases B and C respectively. Fig.3.4 shows the wave-shapes of the applied voltage (Phase A) and the neutral current. In this case, the applied voltage was 11kV, the THD of voltage was 2.49%, V_3/V_1 was 0.44%, V_5/V_1 was 1.98% and V_7/V_1 was 0.30%.

The RMS value of the neutral current is 0.7617 mA. The sum of three 3rd harmonic resistive leakage currents, obtained by the direct method, is 0.8268 mA. Comparing these two, the former is 7.87% smaller.

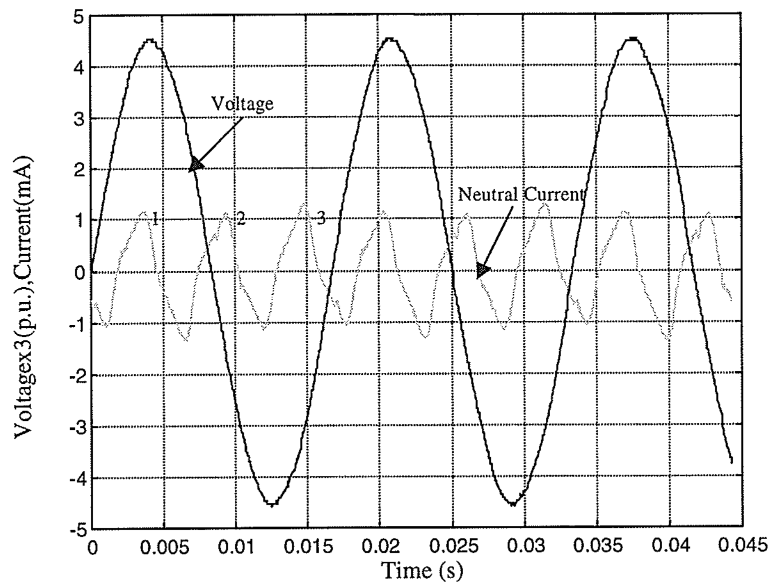

Figure 3.14. Neutral current and applied voltage (11kV) in phase A, MOSA in all three phases unaged

3.5.2. Aged MOSA Set in Phase C, Unaged Sets in the Other Phases

Fig.3.15 shows the wave-shapes of the phase A voltage and the neutral current. The aged MOSA set #04&#06 was inserted in phase C in place of set #09&#11. When the applied voltage was 9 kV, and the RMS value of neutral current was 0.2566mA. As shown in Fig.3.15, the wave shape of the neutral current is obviously distorted. The positive peak value of the neutral current corresponding to the aged set (in phase C) is almost 240° behind the positive peak of the phase A voltage. We know that the MOSA set in phase C is aged. Therefore, peak #3 shown in Fig.3.15 corresponds to the condition of MOSA in phase C.

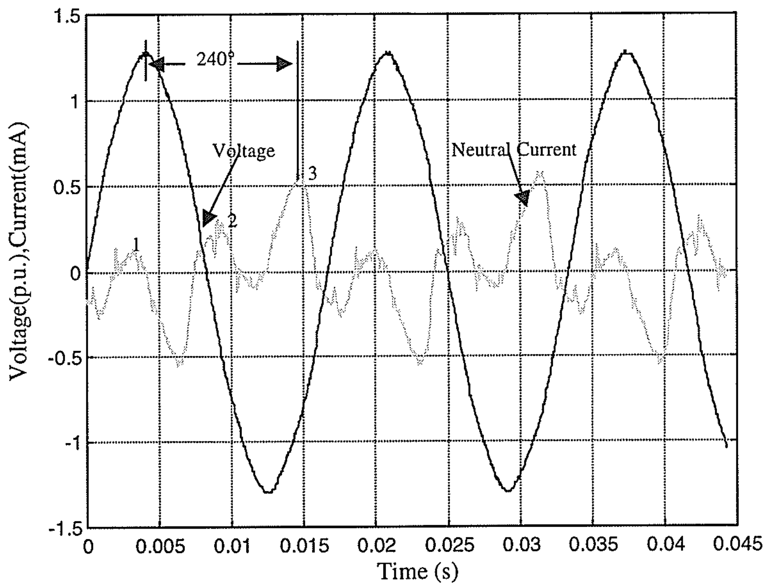

Figure 3.15. Phase A voltage and neutral current with aged MOSA in phase C

Comparing Figs.3.14 and 3.15, it is found that when MOSA in one phase become aged, a larger peak will occur within one cycle (0.1667″) of the voltage and this may be used as an indicator for the condition of the MOSA.

3.5.3. Comments on Neutral Current Method

From Fig.3.14, it is seen that the peak values of the neutral current are not equal because of the slightly non-identical v-i_r characteristics of MOSA. In practice, MOSA in three phases are seldom identical, even if they are unaged. This may result in a misleading judgment. Therefore, for the successful implementation of this method the test results should be compared with test data on an ongoing basis.

If a milliampere meter is connected in the common ground line, as shown in Fig.1.7, the reading of the meter can not show the real condition of the MOSA in the three phases and may cause misleading results. Moreover, if the MOSA in all the three phases age, the usefulness of the reading as a diagnostic indicator is questionable.

3.5.4. Use of Neutral Current Method as a Diagnostic Indicator

From the results of section 3.5.2, it can be concluded that if the MOSA in one phase ages, it results in an increase in one of the peaks of the 3^{rd} harmonic current waveshape in the neutral current. This peak repeats every two cycles at 3^{rd} harmonic frequency. In order for the method to be used as a diagnostic technique, it is necessary to identify the phase in which the aged MOSA is located. For identification purposes, a reference voltage is necessary. However, the reference voltage, which must be taken from a PT or divider, is not so easy to obtain in the field. Without a reference voltage, identification of the aged MOSA is not possible. In order to assess the condition of MOSA in each of the three phases using the neutral current method, a slight modification of this method is necessary. This is discussed in the next section.

3.5.5. Necessary Modification to the Neutral Current Method to Enable its Use as a Diagnostic Indicator

In the following, a modification to the Neutral Current Method is suggested to enable its application on-site as a quick test to determine MOSA condition in a three phase system. The actual implementation of this suggestion is beyond the scope of this thesis but should be considered seriously.

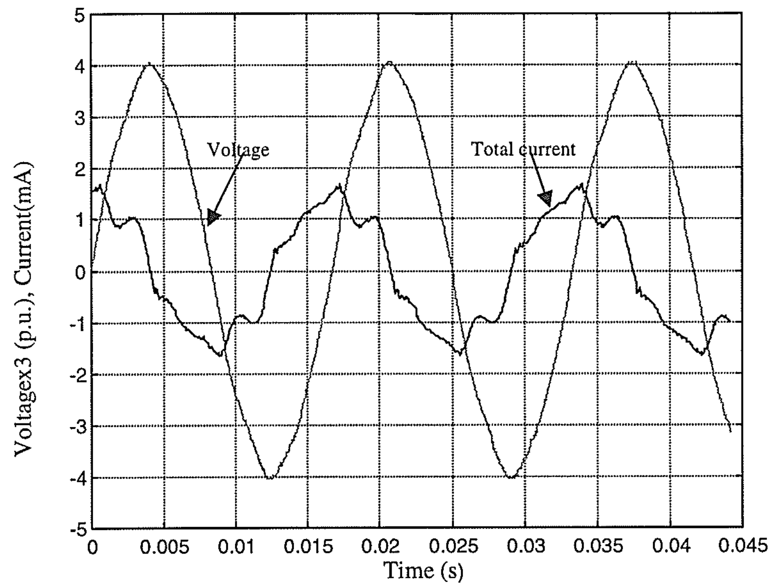

Figure 3.16. The waveshapes of the applied voltage (MCOV) and total current

With the set of MOSA operated at its MCOV, the waveshape of the total current obtained in one phase is shown in Fig.3.16. Because the capacitive current dominates in the low electric field region, it is found that the peak of the total current in each cycle is approximately 90° ahead of the peak of the applied voltage.

We may therefore conclude that in Fig.3.14, for healthy identical MOSA sets, because $I_{r3} >> I_{c3}$, peaks 1,2 and 3 corresponds to phases A, B, and C respectively; the peaks of 3rd harmonic component of the resistive neutral current almost coincide with the peaks of the voltage in each phase.

In Fig.3.15, phase C contains the aged MOSA set. This is the only difference from Fig.3.14. In this figure, peak 3 corresponds to phase C. Although peak #3 is larger, the phase relationship with voltage of phase A is reasonably maintained.

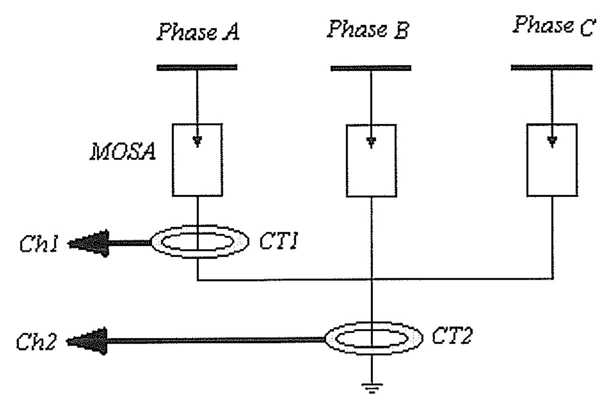

Figure 3.17. Measurements necessary for use of neutral current method as a diagnostic indicator

Therefore, the peak of neutral current identified as "1" in Fig.3.15 is almost 90° behind the leakage current of phase A and the peaks of the neutral current identified as "2" and "3" are 180° and 270° behind the leakage current of phase A respectively. Thus, using suitable CT's simultaneously in one phase and the neutral enables the identification of an aged MOSA during on-site diagnostic test. A test circuit for accomplishing this is shown in Fig.3.17.

CT1 may be inserted in any phase while CT2 (or a shunt) is inserted in the common neutral line. A possible electronic circuit for measurement of the neutral current and indication of the aged phase is shown in Fig.3.18.

In Fig.3.18, the two signals from CT1 and CT2 are first filtered, amplified and sampled through the sampling unit. The sampled signals should then be input into the microprocessor. In the microprocessor, the one phase current and neutral current wave-shapes can be analyzed. The analyzed results can be displayed through a display unit.

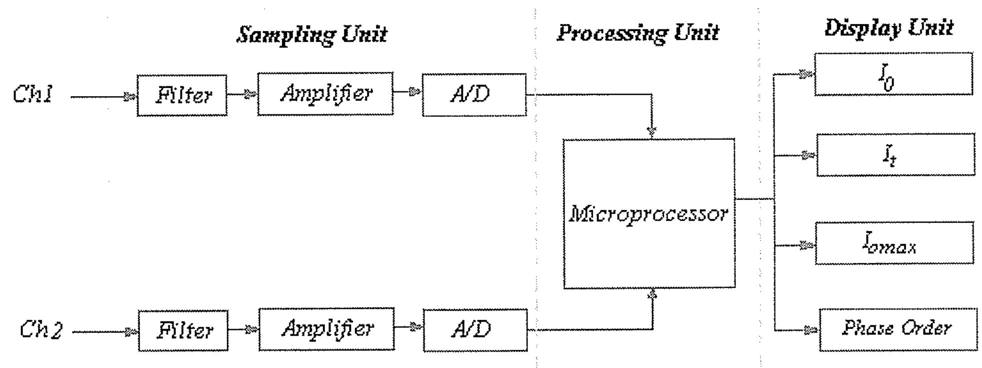

Figure 3.18. Suggested test circuit for the use of the neutral current method as a diagnostic indicator

In the Microprocessor, the neutral current peak values $I_{a(b,c)}$ and the corresponding times of these peaks can be identified within one cycle (0.1667″). Comparing with the peak value of the reference phase current, their phase sequence can be determined. The RMS value of the neutral, I_0, can also be easily calculated. After that, the wave-shape factors, $k_{a(b,c)}=I_{a(b,c)}/I_0$, can also be calculated. The factors $k_{a(b,c)}$ can be displayed. When k_x (x=a,b or c) is abnormal, by comparing these three waveshape factors, the maximum k_x can be displayed and the corresponding phase sequence number can be directly displayed as well.

Thus, with the test circuit and electronic circuit shown in Fig.3.17 and 3.18, it should be possible to obtain the total current and the information about the working condition of the MOSA in each phase.

3.6. Discussion of Electrical Representation Models of MOSA

The simplest representation of MOSA is comprised of a constant capacitance in parallel with a non-linear resistive branch. According to this representation, the resistive current will have the same zero-crossing point as the applied voltage. As shown in Fig.3.7, however, the zero-crossing points of voltage and resistive current are not the same, and its ascending and its descending portions are not symmetrical. These observations indicate that the representation of MOSA by a nonlinear resistor and a pure capacitor is not accurate. Simulation of on-site diagnostic test methods based on this model may result in test errors. In order to investigate this aspect, the test v-i_r characteristic curve of MOSA will be introduced. Using the average v-i_r characteristics obtained in section 3.3.2, benchmark method of section 3.3.2 will be used to obtain the simulated results; these results will then be compared with the experimental results.

3.6.1. v-i_r Characteristics of MOSA from Test Results

Taking MOSA set #04&#6 for example, when the applied voltage is V_N (11kV), the waveshapes of the applied voltage, the capacitive current i_c and the resistive current i_r are shown in Fig.3.19.

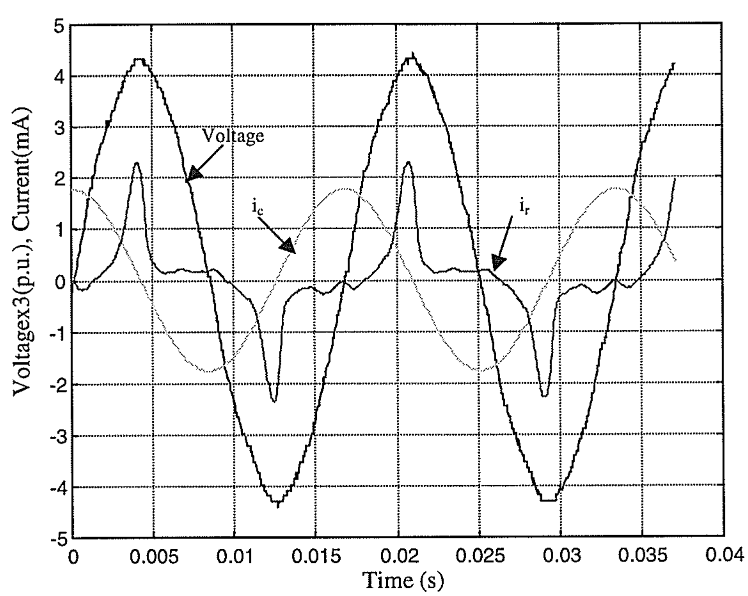

Figure 3.19. Waveshapes of the applied voltage and capacitive and resistive currents

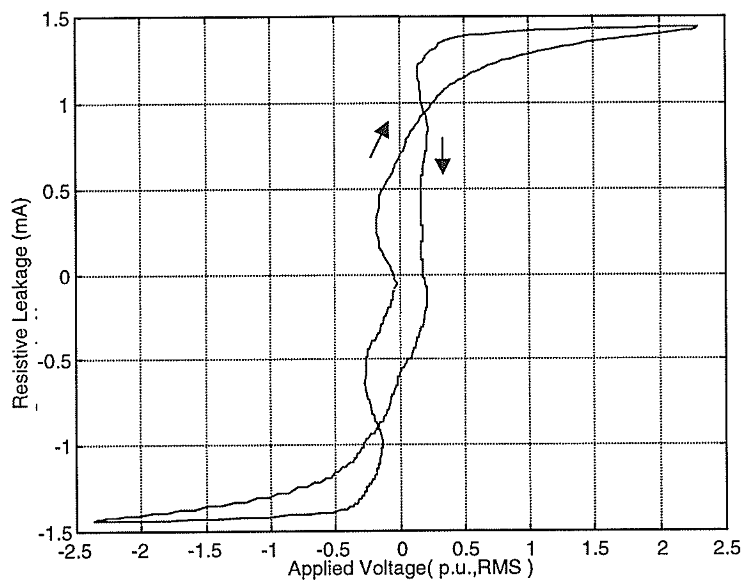

Figure 3.20. v-i_r characteristics of the MOSA from test results

With the v and i_r values obtained from test results, the corresponding v-i_r curve is shown in Fig.3.20. It appears that the characteristic curve of MOSA has some similarities with the B-H relationship of ferromagnetic materials. As we know, ordinary resistors do not display this kind of hysterisis characteristics. Therefore, the simple models are not accurate.

3.6.2. Comparison of Test and Simulation Results, Neutral Current Method

When the MOSAs in the three phases are unaged, the measured voltage and neutral current waveform are as shown in Fig.3.21. Appling FFT to the measured voltage, the harmonic voltages were calculated. With the experimentally obtained average v-i_r characteristic curve of Fig.3.9, the simulated neutral current was calculated and its wave-shape is shown in Fig.3.21 as well. These waveforms were obtained with MOSA sets #10&#14, #02& #16 and #09&#11 in phases A, B and C respectively. The applied voltage is 10kV.

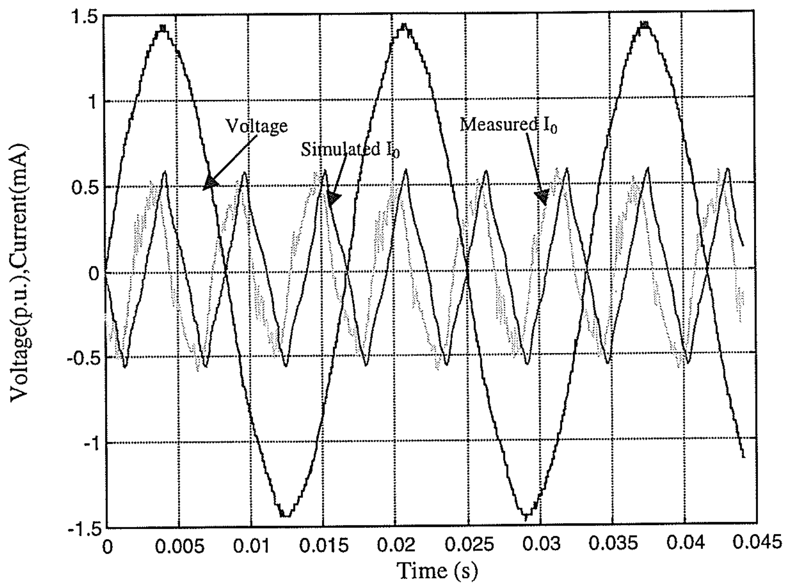

Figure 3.21. Waveshapes of simulated and measured neutral currents of unaged MOSA in a three phase system

The measured neutral current is 0.3382 mA, while the simulation yields a value of 0.3294 mA. The error in the simulation result is 2.60%.

Next, the MOSA set in phase C was replaced with an aged one, i.e. #04&#06; 9kV was applied, the measured wave shapes of the applied voltage and neutral current are shown in Fig.3.22. Using the average v-i_r characteristic curve (Fig.3.9) of the aged MOSA for the simulation of Phase C and the average v-i_r characteristic curve of the unaged MOSA (Fig.3.9) for other two phases, the simulated waveshape of neutral current was obtained. This is shown in Fig.3.22 as well.

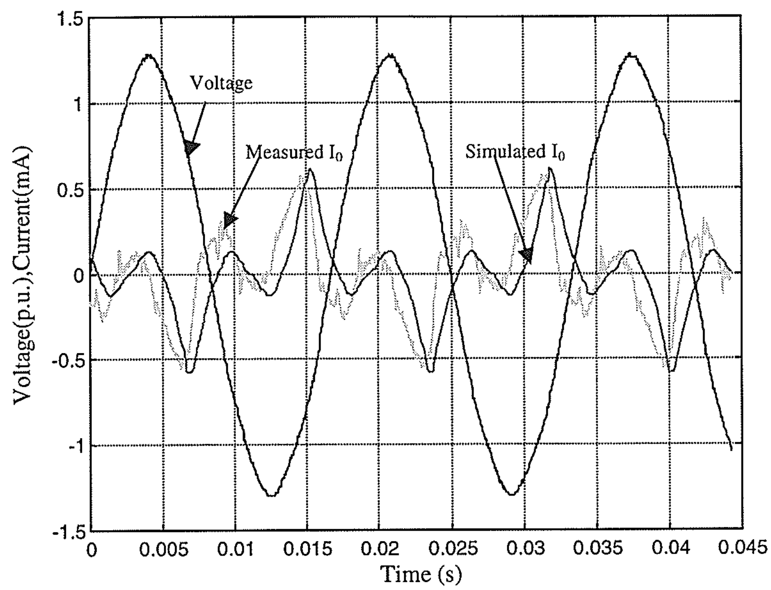

Figure 3.22. Measured and simulated neutral currents with aged MOSA in phase C

In this case, the measured neutral current is 0.2566mA. The simulated result is 0.2404 mA. The error in the simulation result is 6.31%.

3.6.3. Effect of MOSA Representation on Simulated Results

In section 3.6.2, the test and simulated neutral current waveshapes were shown in Figs. 3.21 and 3.22. Because of the hysterisis characteristics of MOSA, the simulated and the test waveshapes show some differences.

The zero crossings of the neutral current in the test and simulated results are different. This shows that using a non-linear resistor to represent the hysteretic characteristics of MOSA is inaccurate.

The magnitudes of the simulated neutral current and the test result are almost equal. Use of the simplified MOSA representation model, as shown in Fig.3.4, for simulation can satisfy the requirements in those cases where the precision requirement is not so high.

Chapter 4

Conclusions

4.1. Conclusion

In this thesis, the v-i_r characteristics of MOSA and existing on-site diagnostic techniques of MOSA are briefly reviewed. In Chapter 2, the representation models of MOSA are discussed first, followed by a discussion of the influence of harmonic voltages, their magnitudes and phase angles, on the resistive leakage current and its 3^{rd} harmonic component, which are often used as diagnostic indicators. This was done by computer simulation using the real v-i_r characteristic curves of aged and unaged MOSA. In Chapter 3, the v-i_r characteristics of MOSA sets used in the experiment were obtained with the compensation method. Improvements in the compensation method have been suggested for field use. For the probe method introduced in [3], with a three-phase setup, it is shown that errors introduced are dependent on probe position. For the Neutral Current method, the neutral current with aged and unaged MOSA sets were obtained. Based on the test results, modifications to this method have been suggested which will enable its application to on-site diagnostic tests of MOSA. Finally, based on the test v-i_r characteristic curves of MOSA, the electrical representation of MOSA is discussed; and the results obtained from the simulation using the existing representation model of MOSA are compared with the test results.

The following conclusions may be drawn from the study in this thesis:

(1) The magnitude and phase angle of the harmonic voltages will greatly influence the measurement of the resistive leakage and its 3rd harmonic component, which are taken as indicators for the condition of MOSA. Neglecting the voltage harmonics in an on-site diagnostic test of MOSA will lead to misleading results.

(2) The 3rd harmonic component of the resistive leakage current, which is taken as the indicator in the probe method, is also influenced by the position of the probe. The assumption of a constant field factor in the probe method will result in test errors.

(3) The compensation method, which takes the resistive leakage current as the indicator, may be improved for on-site use, if a new criteria and a soft phase shifter, as proposed in this thesis, are used to eliminate the influence of harmonic voltages and interphase interference.

(4) The neutral current method, with its simplicity and convenience of use, may be improved for on-site use by introduction the measurement of one phase leakage current. To achieve this goal, the test circuit proposed in this thesis could be implemented.

(5) Test v-i_r characteristic curves show that the representation models of MOSA are not accurate. This will result in some errors in simulations.

4.2. Recommendations for Future Research

This thesis offers the following suggestions for future work:

(1) A further investigation of the v-i_r characteristics of MOSA and the presently used electrical representative methods on the on-site test results, especially for those currently used techniques.

(2) The investigation of character of the leakage current from the surface of MOSA housing, especially under pollution.

(3) The realization of the improved neutral current method as proposed in this thesis.

(4) Further study of the influence of system harmonic voltages on the resistive leakage current for on-site test purposes.

References:

1. A.Schei et K.H.Weck, " Metal Oxide Surge Arresters in AC Systems Part1: General properties of the metal oxide surge arretser",Electra, N° 128, 990, p100-105

2. Kazuo Eda, " Conduction Mechanism of Non-Ohmic Zinc Oxide Ceramics", J. Appl. Phys. 49(5), 1978, p2964-2972

3. J.Lundquist, L.Stenstrom, A.Schei, B.Hanson, "New Method for measurement of the Resistive Leakage Current of Metal-Oxide Surge Arresters in Service", IEEE Trans. on PWRD, Vol. 5, No.4, 1990, p1811-1822

4. Zhang Yan, On-line Monitoring of Electrical Insulation, Electric Industry Publish of China, 1997

5. Yue Chang, Jiali Qian, "Analysis on Resistive Leakage Current of ZnO Surge Arresters Detected LCD-4 Instrument, Single Phase", High Voltage Techniques (Chinese), Vol.21, No.2,1995, p77-80

6. Yue Chang, Jiali Qian, "Analysis on Resistive Leakage Current of ZnO Surge Arresters Detected LCD-4 Instrument, Three Phase", High Voltage Techniques (Chinese), Vol.21, No.4,1995, p35-36

7. Yimei Jia, Fuheng Xu, " Methods to Measure Leakage Current of ZnO Arresters On-line", Journal of Wuhan University of Hydraulic and Electric Engineering, 1995, p30-35

8. H.R.Philipps, Lionel M. Levison, " Low-temperature Electrical Studies on Metal-Oxide Varistors – A Clue to Conduction Mechanisms", Journal of Applied Physics, Vol. 48, No.4,1977, p1621-1627

9. A. Bargigia, L.Giannuzzi, " Study of the Performance of Metal Oxide Arresters for High Voltage Systems", 33-14, CIGRE, International Conference on Large High Voltage Electric System, Vol. II, 1986

10. M.R.Raghuveer, Power Transmission Lines, Chapter 6, p10

11. J.Arrillaga, D.A.Bradley, P.S.Bodge, Electric Power Systems Harmonics, New York: Wiley c1985